RSC Sustainability

ROYAL SOCIETY OF CHEMISTRY

PAPER

View Article Online
View Journal | View Issue

Cite this: *RSC Sustainability*, 2024, **2**, 3525

Utilization of green resource-based *Mimosa pudica* hydrogel powder in a cellulose acetate-based polymeric membrane as absorbent: a sustainable approach towards female hygiene application†

Roshni Pattanayak,[ab] Sukanya Pradhan[a] and Smita Mohanty *[a]

This study presents the development of a novel membrane-based absorbent by incorporating *Mimosa pudica* hydrogel (MPH) powder, derived from the mucilage of its seeds, into a cellulose acetate polymer matrix using the non-solvent induced phase separation (NIPS) method. The membranes were prepared with varying weight percentages (wt%) of MPH to evaluate their potential as absorbent cores for hygiene products. The enhanced absorbency observed for 1 wt% MPH-loaded cellulose acetate membrane (MCA-2) was attributed to the MPH powder's large surface area and macroporous structure, as confirmed by Brunauer–Emmett–Teller (BET) analysis. The MCA-2 membrane exhibited maximum absorbency values of 276.66%, 402.87%, and 572.5% in distilled water, 0.9 wt% saline solution, and defibrinated sheep blood, respectively, within 30 minutes along with an absorbency under load value of 439.69% in saline solution at 60 minutes. An in-depth analysis of the thermal, mechanical, morphological and topographical properties of the developed membrane was conducted. This exhibited a modulus value of approximately 120 ± 0.5 MPa with 13.07 ± 0.2% elongation and also possessed significant antibacterial properties against *E. coli* and *S. aureus* bacteria justifying its potential as an absorbent core. Additionally, 16S rRNA sequencing was performed to identify bacteria involved in soil burial degradation, highlighting its overall impact and sustainability towards the environment. These findings suggest that MPH-incorporated membranes hold significant promise as absorbent materials in female hygiene applications.

Received 16th July 2024
Accepted 24th September 2024

DOI: 10.1039/d4su00381k

rsc.li/rscsus

Sustainability spotlight

The commercially available petrochemical acrylate-based female hygiene products adversely affect both female health and the environment. To address this issue, current research focuses on the development of a cost-effective biobased formulation which can be a sustainable alternative and solution to this targeted application. The modified cellulose acetate membrane incorporated with *Mimosa pudica* hydrogel (MPH) powder not only exhibits a prominent antibacterial efficacy against *E. coli* and *S. aureus* bacteria but also has a high absorbency justifying its potential to be utilized as a core in a feminine hygiene product. Moreover, degradation analysis using 16S rRNA sequencing provides a clear vision of the developed sample that addresses the Sustainability Goals (SDG 3: good health and well-being; SDG 12: sustainable consumption and production; and SDG 15: life on land).

1. Introduction

Commercial hygiene products based on polyacrylates and their derivatives absorb more liquid than their initial weight making them an ideal material for wider applicability in female hygiene products.[1,2] The bleached cotton/material used in the absorbent core of a hygiene product also contains more acrylate-based synthetic superabsorbent materials, dioxins, volatile organic compounds and phthalates, which have been the primary causes of various health issues, including skin allergies, carcinogenesis and reproductive tract infections (RTIs).[3–5] In addition, each hygiene product contains two grams of nonbiodegradable plastic, which takes 500–700 years to completely degrade, generating abundant municipal waste every year. Approximately 12.3 billion tons of sanitary napkins are disposed of in landfills, which adversely affects the environment.[6] Moreover, incineration of these products releases dioxins, furans and carbon dioxide into the atmosphere, thereby influencing the increase in air pollution.[7,8] These facts have resulted in increased global consciousness and considerable research efforts in the design

[a]*School for Advanced Research in Petrochemicals (SARP), Laboratory for Advanced Research in Polymeric Materials (LARPM), Central Institute of Petrochemicals Engineering & Technology (CIPET), Patia, Bhubaneswar, Odisha, 751024, India. E-mail: drsmitamohanty@gmail.com*

[b]*Utkal University, Vani Vihar, Bhubaneswar, Odisha, 751004, India*

† Electronic supplementary information (ESI) available. See DOI: https://doi.org/10.1039/d4su00381k

and development of numerous biobased formulations using various techniques.[9–12]

The phase inversion technique has been the most versatile cost-effective technique for preparing polymeric membranes, tailor made for a wide range of applications in micro- or ultrafiltration,[13] paint and coatings,[14] pharmaceuticals,[15,16] cosmetics,[17] textiles,[18] and production of various industrial products. These methods are generally divided into four categories based on their controlling process parameters: nonsolvent-induced phase separation (NIPS), thermal-induced phase separation (TIPS), vapor-induced phase separation (VIPS) and evaporation-induced phase separation (EIPS). The NIPS technique is a well-established, inexpensive membrane preparation process in which a polymeric solution is cast on a suitable glass plate using a membrane casting unit. The cast solution plate is then immersed in a coagulation bath filled with nonsolvent to prepare a porous membrane.[19,20] During this process, mass transfer and diffusion between the solvent and antisolvent occur across their interface, introducing phase separation of the polymeric solvent to solidification (or precipitation). These materials create more porous structures throughout the surface that can absorb larger amounts of liquid when immersed in various liquid media. NIPS is suitable for developing a low-cost hygiene-absorbent material which can be placed in the middle layer of a sanitary napkin. Reshma *et al.*[21] developed a newly formulated sodium carboxymethyl cellulose membrane using aluminium sulfate and sodium trimetaphosphate chemical crosslinking agents for female hygiene applications. Here, the authors used two membrane fabrication techniques, *i.e.* phase inversion and lyophilization, separately to develop the samples for a comparative analysis. The phase-inversed membrane showed significant porous structure, structural stability and better sorption to blood solution. The efficiency of this cost-effective green method provides a promising substitute for mass production of products.[22,23]

Cellulose-based materials have attracted considerable research interest because of their inherently available hydroxyl groups that permit more liquid absorption without harming the human body.[24,25] Among all cellulose-based materials including cellulose nitrate, carboxymethylcellulose, methylcellulose, ethylcellulose, and sodium carboxymethylcellulose, cellulose acetate, a typical bioderived polysaccharide, has been the most abundant, nontoxic, easily viable, low-cost, biodegradable, biocompatible and renewable polymer.[26,27] Yadav *et al.*[28] have designed an electrospun cellulose acetate that showed immediate sorption with 1200–1400% water absorption along with higher mechanical stability and ease in processing, which contributed to wider applicability. Besides this, cellulose acetate is easily soluble in various solvents, such as *N*,*N*-dimethylacetamide and dimethylformamide,[25] which can be suitably utilised to prepare membranes using NIPS techniques.

Renewable resource-based superabsorbent polymers (SAPs) can be suitably used in the development of composite membranes to enhance their overall performance.[29] Various alternative natural SAPs derived from orange peels, avocado peels,[30] chia seeds,[31] chia flours, *etc.*, have been proposed by many researchers for use in female hygiene products (sanitary napkins) to overcome the problems associated with synthetic petroleum-based SAPs.[32] *Mimosa pudica*, also known as touch-me-not flower plant, lajwanti or shame plant, belongs to the Mimosaceae family and is an annual or perennial shrub commonly found in tropical regions of Brazil, Asia, America, Nigeria, and some Pacific islands. It is also abundantly found in the tropical and sub-tropical parts of India due to its adaptability to various climatic conditions. All the parts of this plant, including roots, leaves, flowers, and seeds, possess considerable medicinal value and have been extensively used in ayurvedic science for curing many diseases, such as constipation, ulcers, snake bites, depression, and skin and respiratory diseases. This therapeutic potential is attributed to its rich phytochemical content including alkaloids, sterols, terpenoids, tannins and flavonoids within it.[33–35] Despite its extensive medicinal use, various research studies have been conducted only on the leaves and roots of the *Mimosa pudica* plant for drug delivery, wound healing and pharmaceutical applications.[36–41] However, *Mimosa pudica* seeds are rich in glucuronoxylan and have the capability of accumulating more liquid during immersion and subsequent formation of three-dimensional hydrogel structures. *Mimosa pudica* hydrogel (MPH) needs to be explored for its viability as a potential candidate for SAP. According to a study by Aziz *et al.*,[42] a *Mimosa pudica* plant is able to produce approximately 675 seeds per year. These seeds are readily available from local nurseries, herbal stores and local e-commerce vendors, typically costing between 50 and 200 INR per packet. This affordability and ease of access make this plant a viable option for large-scale production, with minimal maintenance cost. Its low maintenance requirements and adaptability further support large-scale cultivation, though efficient processing methods are crucial for scaling up its large-scale industrial production. Besides this, these seeds show a greater swelling value at pH 6.8–7.4, whereas this value is lower at pH 1.2.[43] A hydrogel mucilage can be easily extracted from *Mimosa pudica* seeds when they are soaked in water which can be then dried and ground into powder for further analysis. Thus, combining MPH in powdered form within a biodegradable polymer can suitably provide a sustainable product bestowed with improved absorbency as well as antibacterial characteristics. Overall, the affordability and availability of *Mimosa pudica* seeds and their low processability cost support their potential for widespread use in sustainable material development.

The current study focuses on developing a sustainable, biobased absorbent core for female hygiene products through a novel porous composite membrane composed of cellulose acetate and powdered MPH using the NIPS technique. An in-depth analysis of the mechanical and thermal properties of the composite membranes was undertaken. Additionally, BET surface area and pore size measurement as well as X-ray diffraction (XRD) were performed on the MPH powder for a more comprehensive analysis. Morphological studies were carried out using a scanning electron microscope (SEM) and atomic force microscope (AFM) to determine the porosity and surface roughness of *Mimosa pudica* seeds, MPH powder as well as composite membranes. The antibacterial efficiency against *E.*

coli and *S. aureus* bacteria has also been evaluated along with a biodegradability study using the soil burial method. Furthermore, 16S rRNA sequencing was employed to analyse the bacterial population involved in the degradation process, providing insight into the decomposition mechanism. Overall, the novelty of this research involves developing a cost-effective, sustainable and efficiently antibacterial biobased composite membrane. By incorporating natural MPH filler into a cellulose acetate matrix, this novel composition as an absorbent core offers significant benefits for both female health and environmental sustainability.

2. Materials and methods

2.1. Materials

Cellulose acetate (CA) (M_n = 50 000) was purchased from M/s Sigma Aldrich, India. Acetone (99.9% pure) and *N*,*N*-dimethylacetamide (DMA) were purchased from M/s Merck India. *Mimosa pudica* seeds were bought from a local e-commerce store and further processed to produce MPH powder. Mueller–Hinton agar powder used in the antibacterial test was procured from M/s Himedia, India. The soil used for the soil burial test was obtained from a laboratory campus. Deionized water was prepared in the laboratory and used throughout the experiment. Anticoagulant-defibrinated sheep blood was procured from M/s S. R. Group, New Delhi and stored at 2–8 °C. Sodium chloride was used to prepare the 0.9 wt% saline solution.

2.2. Methods

2.2.1. Preparation of MPH. *Mimosa pudica* seeds were thoroughly washed under running tap water until clean. The seeds were then soaked in distilled water for 12 h, resulting in the formation of hydrogel. After soaking, the excess water was drained, and the soaked seeds were transferred to a round-bottom flask which was placed in a water bath and stirred at high speed for 30 min at a temperature of 50 °C. The hydrogel was then put in boiling water for 5 minutes to remove lipophilic compounds. Following this, the gel-like mucilage released from the *Mimosa pudica* seeds was dried in an oven at 50 °C for 30 minutes to remove excess water, and the weight was recorded until three consistent consecutive weights were achieved. The mucilage was then ground using a centrifugal mill at 18 000 rpm, ensuring complete separation from water. To ensure complete drying, the mucilage was further dried at 50 °C for five days and was then scraped from the Petri dish and crushed using a mortar and pestle. The dried mucilage was then passed through a sieve shaker to obtain fine powder of various sizes, including 90, 120, and 150 μm. This fine powder was collected and stored in an air-tight container at room temperature to prevent particle humidification. This procedure for isolating MPH powder was adapted from the method reported by Peng *et al.*,[43] with some minor modifications in rpm and temperature tailored to meet the specific requirements of the experiment. The procedure is pictorially illustrated in Scheme 1.

2.2.2. Preparation of membrane through NIPS method. Initially, CA powder was dissolved in a mixture of acetone and *N*,*N*-dimethylacetamide at a 2 : 1 ratio to prepare CA solution at variable concentrations of 2.5 wt%, 5 wt% and 10 wt%. The solution was stirred for 14–16 hours at room temperature until it became transparent and clear. Subsequently, sonication was performed for approximately 60 minutes for the complete preparation of the solution. The prepared solution was then kept at room temperature without being stirred to allow the

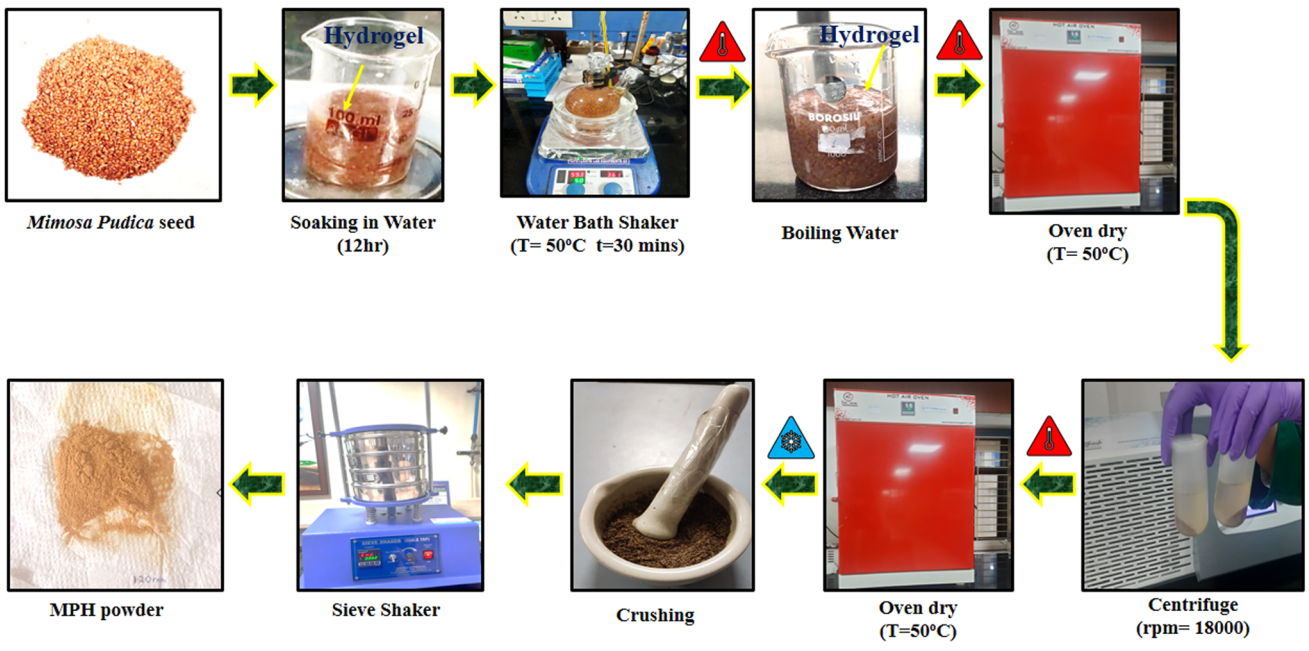

Scheme 1 Pictorial representation of MPH powder preparation.

Table 1 Details of the compositions for all developed samples

No.	Sample code	Cellulose acetate (CA) concentration (wt%)	MPH concentration (wt%)
1	Neat CA	5	0
2	MCA-1	5	0.5
3	MCA-2	5	1
4	MCA-3	5	2

residual bubbles to escape. Membrane casting equipment (M/s Tech Inc, Chennai, India) was used to cast the membranes while using water in the coagulation bath as an antisolvent. The developed membranes were finally dried for 24 hours in a desiccator. The membrane with 2.5 wt% of neat CA disintegrated while the amount of solute used for casting was insufficient to form the required viscous solution. Therefore, CA contents of 5 wt% and 10 wt% were considered for further analysis. Subsequently, MPH/CA composite solution (MCA) at a variable concentration of 0.5 wt%, 1.0 wt% and 2 wt% of MPH in 5 wt% CA solution was prepared at 750–800 rpm at room temperature. The composite solution was then cast onto the same membrane casting unit which was then kept in the coagulation bath and finally dried for 24 hours. The resulting modified cellulose acetate membranes were designated as MCA-1, MCA-2 and MCA-3, corresponding to the addition of 0.5 wt%, 1 wt% and 2 wt% MPH in the neat CA sample, respectively, as outlined in Table 1. The procedure is schematically illustrated in Scheme 2.

2.3. Characterization techniques

2.3.1. Chemical analysis. Spectroscopic analysis of the developed membranes was conducted using a Smart Orbit ATR Nicolet 6700 Fourier transform infrared (FTIR) spectrometer (M/s ThermoFisher, USA) in the wavenumber range of 4000–500 cm^{-1} with a resolution of 4 cm^{-1} and an accuracy of 0.1% transmission at room temperature.

2.3.2. BET–BJH surface area and pore size analysis. The developed MPH powder of particle size of 90, 120 and 150 μm was analyzed using N_2 physisorption with a Microtrac Belsorp Max G instrument, Japan (BEL Control Version 1.4.1) to determine the BJH (Barrett–Joyner–Halenda) pore size and Brunauer–Emmett–Teller (BET) surface area. Samples of approximately 250 mg were taken for the analysis which were initially preheated in an inert atmosphere at a temperature of 80 °C for 120 min with a ramping rate of 5 °C min^{-1}. Here the initial vapour pressure was 10 kPa and the saturation vapour pressure was maintained at 109 kPa throughout the experiment. After completion of pretreatment, samples were subjected to surface area analysis in liquid nitrogen atmosphere for complete analysis.

2.3.3. Free absorbency. The absorbing capacity of the prepared membrane was determined in accordance with the ASTM D 570 standard.[44] The primary purpose of the determination of absorbency is to measure the amount of liquid absorbed by the samples within a specific time, such as 10 s, 1.5 min, 10 min, 15 min, 30 min, 60 min, 180 min, 360 min and 1440 min. The test was performed using 100 mL of distilled water, 0.9 wt% saline solution and defibrinated sheep blood (procured from M/s S. R. Group, New Delhi) medium. Prior to the initiation of the test, the samples were predried in a desiccator for 24 hours, and the absorbency test was performed as described previously.[44] Each test was repeated three times and the data reported as the average of three measurements. The absorbing capacity was calculated using eqn (1):

$$\text{Absorbency percentage (\%)} = (w_2 - w_1)/w_1 \times 100 \quad (1)$$

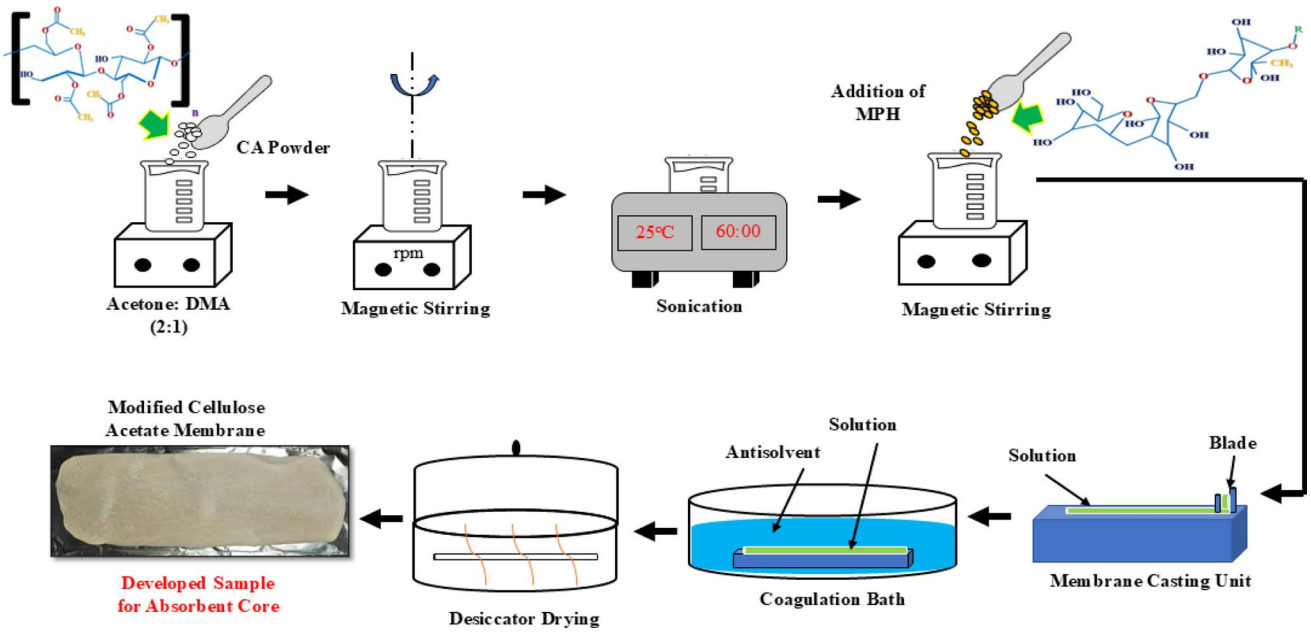

Scheme 2 Schematic illustration of modified cellulose acetate (MCA) membrane preparation using NIPS method.

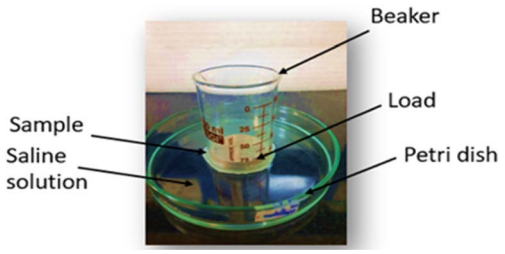

Scheme 3 Schematic illustration of an experimental setup for the AUL test.

Where w_1 is the weight of the dry sample and w_2 is the weight of the wet sample.

2.3.4. Absorbency under load (AUL) (AUL test). This test was performed to determine the absorbency capacity of the sample after a load was applied, and 0.9 wt% saline solution was used to perform the test. In this test, the absorption capacity, strength, and stability of the prepared membrane were measured after applying a certain load to the absorbent core of a sanitary napkin. The schematic setup for the AUL test is shown in Scheme 3. The sample was cut into a circular shape of 30 mm in diameter and weighed as w_1. Prior to performing the test, the samples were dried in a desiccator for 24 h for complete drying. The initial weight of the sample was recorded as w_1. The sample was kept in a clean Petri dish, and a load of 90 g was applied, as shown in Scheme 3. After that, the saline solution was poured into the Petri dish, and the AUL test was performed for 60 minutes. The sample was then removed from the applied load, and the final weight was measured after 60 minutes of absorption (w_2). The absorbance under a load of membrane samples was calculated by using eqn (2):

$$\text{Absorbency under load (AUL, \%)} = (w_2 - w_1)/w_1 \times 100 \quad (2)$$

2.3.5. XRD analysis. XRD analysis was performed using an X-ray diffractometer (M/s Shimadzu, XRD-7000 L, Japan) with a scanning rate of 5 deg per min and a scanning angle 2θ range of 2°–80°. The instrument used Ni-filtered Cu-Kα radiation from an X-ray beam ($\lambda = 0.1546$ nm) and operated at a power of 40.00 kV and current of 30 mA.

2.3.6. Morphological analysis. The surface morphology of the samples was analysed using field emission scanning electron microscopy (FESEM) (M/s Zeiss, Gemini SEM 300, UK) with an accelerating voltage of 5 kV at different magnifications. For each analysis, the surface of the membrane was sputtered with a gold–palladium mixture. Further, SEM micrographs, (EVO MA 15, Carl Zeiss smt, Germany) were obtained for the MPH powder for additional analysis.

2.3.7. Topographical analysis. The topography of the samples was visualized with an AFM (XE-100, M/s Park-South Korea) in non-contact mode where the surface roughness of the porous structure was measured.

2.3.8. Mechanical analysis. A developed membrane sample (6 cm × 2 cm × 0.015 cm, measured by a digital micrometer) was subjected to tensile testing with a universal testing machine (M/s Instron 3382, Massachusetts, USA) at room temperature, and stress was applied at a rate of 3 mm min^{-1}. A total of three replicates were tested for each sample to ensure the reproducibility and repeatability of the result and the standard deviations have been included in the result section.

2.3.9. Thermal analysis. Thermogravimetric analysis was performed in the temperature range of 25–800 °C with a TGA (Q50, M/s TA Instruments, USA) instrument in an inert nitrogen atmosphere with a heating rate of 10 °C min^{-1}.

2.3.10. Antibacterial analysis. The antibacterial activities of neat CA, freshly developed MCA-2 formulation and six-month-old MCA-2 were tested against *Escherichia coli* (Gram negative) and *Staphylococcus aureus* (Gram positive) using a disc diffusion method. Briefly, agar medium was prepared and poured into glass plates for solidification under UV light. After that, a bacterial suspension of 10^6 CFU mL^{-1} was inoculated evenly across the respective plates. The samples were placed in a plate and kept frozen for 1 h of drying for proper diffusion. Then, the plate was incubated for 24 hours at 37 °C. Subsequently, the inhibition zone around each sample was measured to quantify the antibacterial properties in the developed composition.

2.3.11. Soil burial test, ecotoxicity test and identification of bacteria through 16s rRNA sequencing. Biodegradation was performed using the soil burial method according to previous methods.[43] In brief, the soil collected from our institute's garden campus was used for this test, which had a C/N ratio of approximately 12.9. The developed samples were cut into 2 cm × 2 cm pieces and tested to determine their degradability. They were buried 3 cm below the surface of the container, which was filled with garden soil. Afterwards, more soil was poured into the container until the entire sample was covered. These samples were covered with aluminium foil and kept at room temperature, and the moisture content was properly maintained in the range of 30–35% on a regular basis. The samples were removed every 60 days, and morphological analysis was performed to determine the degradation behaviour of the samples. Additionally, an ecotoxicity test was conducted to examine the impact of the degradation process on the soil's ability to support plant growth. Following the OECD 208 guidelines,[49] the emergence of Moong seedlings in soil containing the membrane samples (neat CA and MCA-2) was compared to that in blank specimens. The overall morphology of the grown plants and the effect on biomass were also observed to evaluate the impact of sample degradation on plant growth. Moreover, microorganisms present in the degraded sample were identified by a pure culture technique. Briefly, the soil material present on the surface of the degraded membrane was collected through a sterilized cotton swab very carefully and further processed for the isolation of genomic DNA by growing individual bacterial colonies in culture media. The prepared plate was stored in the dark at room temperature, and microbes were quantified by morphological observation. This experiment was carried out in triplicate, and the average values are reported here. Gram staining was used to identify the microorganisms and differentiate between bacterial species based on their cell wall composition. The resulting genomic DNA was used for amplification of the 16S rRNA gene *via* polymerase chain reaction (PCR),

and the amplified rDNA samples were subsequently sequenced using 16S ribosomal RNA primers. The obtained sequencing data were analysed, and the identified bacteria were confirmed by the GenBank database BLAST (blastn) 2.2.24 program[45] by comparison by matching up to 95–97% similarity.[46–49]

2.3.12. Mold growth resistance analysis. A mold growth resistance test was performed to evaluate the amount of mold growth around the material in a moist atmosphere according to a previous study.[50] Membrane samples of 2 cm × 2 cm were cut and placed in a clean Petri dish and were kept in an airtight plastic container with 50 mL of distilled water at the bottom, as shown in ESI 1.† Additionally, the absorbent core of a commercial sample, Stayfree Secure Wings sanitary napkin consisting of cellulosic fiber, hydrocarbon resins, naphthalic oil, TiO_2, polyethylene, and calcium salts of fatty acids, was carefully removed from a single napkin, cut to the same sample size and used as a reference for the experiment.

3. Results and discussion

3.1. Chemical analysis

Fig. 1(a) shows the FTIR spectra of neat CA membranes, at variable compositions of 2.5 wt%, 5 wt% and 10 wt%, whereas Fig. 1(b) depicts the molecular fingerprint spectra of optimized neat CA at 5 wt% and its corresponding modified CA membranes formed with variable concentrations of MPH powder. In this case, an IR spectrum in the 4000–500 cm^{-1} region was employed to analyse the absorption bands and identify the functional groups present in the sample with changes in peak intensity relative to wavenumber variation. The absorption peaks were attributed to the presence of more hydroxyl (–OH) groups, around 3475 cm^{-1}, in all samples. The characteristic C–H stretching vibration of methyl groups ($-CH_3$) was observed around 2929 cm^{-1} confirming the presence of cellulose acetate in the prepared membranes.[27] Furthermore, FTIR spectra of *Mimosa pudica* seed and our developed MPH powder are illustrated in Fig. 1(c). Here, the –OH stretching vibration was observed at 3280 cm^{-1} due to the presence of phenolic compounds, and –CH stretching and C=O stretching vibration bands were recorded at 2930 cm^{-1} and 1638 cm^{-1} respectively. An additional carbonyl (C=O stretching) band arises at 1743 cm^{-1} in the developed powder as mucilage primarily exhibits glucuronoxylan which predominantly contains glucuronic acid and D-xylose as its main constituents. The presence of aromatic amino groups was confirmed in a range of 1650–1350 cm^{-1}. As a whole, due to the manifestation of hydroxyl and carbonyl groups adhered to the mucosal surfaces to mucilage form, FTIR spectra were inclusively intensified for the developed

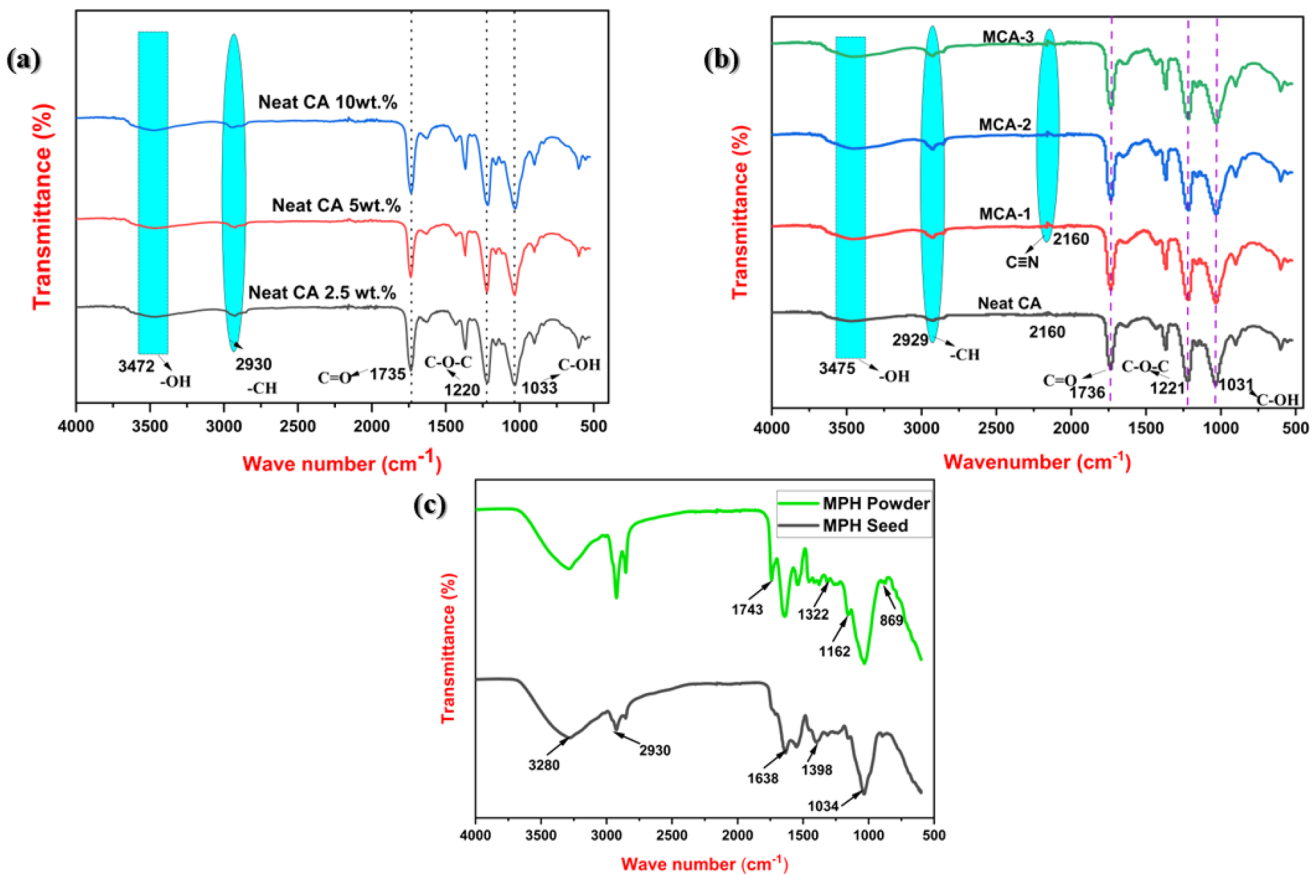

Fig. 1 (a) FTIR spectra of neat CA membranes at various compositions of 2.5 wt%, 5 wt%, 10 wt%. (b) FTIR spectra of neat CA at 5 wt% and its corresponding modified CA membranes formed with variable concentrations of MPH powder (MCA-1:0.5 wt% MPH powder loaded modified CA membrane, MCA-2:1 wt% MPH powder loaded modified CA membrane, MCA-3:2 wt% MPH powder loaded modified CA membrane). (c) FTIR spectra of *Mimosa pudica* seed and developed MPH powder.

powder as compared to the MPH seed. Moreover, after the incorporation of MPH powder, the C–H absorption peak progressively got intensified as filler concentration increased in all modified membranes. This may arise due to the presence of essential biocomponents including flavonoids, terpenoids, sterols, tannins and alkaloids in the MPH powder. An additional peak also appeared at 2160 cm^{-1} in the modified samples which is the consequence of the interaction between the cellulose backbone and the nitrile group of protein content following the inclusion of these bio-fillers.[51] The characteristic peaks around 1736 cm^{-1}, 1431 cm^{-1}, 1221 cm^{-1}, and 1031 cm^{-1} were observed for the neat CA samples which confirmed the presence of carbonyl group stretching (C═O), CH_2 deformation vibration, –C–O–C– antisymmetric stretching of ester group and –C–OH– stretching vibration respectively. Marginal shifting and lower intensity vibration peaks were noticed which is primarily due to the interaction of MPH with the CA thereby creating a complexation effect in the CA/MPH membrane. The presence of both –C–O stretching and –CH_2 rocking vibrations is responsible for the presence of a peak around 901 cm^{-1}. A complete glimpse of a strong interaction between the cellulose acetate and filler was confirmed in this study.[52] The molecular vibration modes and their corresponding wavenumbers for neat CA, modified CA, *Mimosa pudica* seeds and MPH powder are tabulated in Tables 1 and 2(a) and (b) in ESI 1.†

3.2. BET–BJH surface area and pore size analysis

The MPH powder of various mesh sizes of 90, 120 and 150 μm was characterized *via* BET adsorption–desorption isotherm, as well as BJH pore size measurement, as shown in Fig. 2. All the BET surface area measurements and pore size and volume are summarized in Table 2. The specific surface areas of MPH powder with mesh sizes of 90 μm, 120 μm, and 150 μm were found to be 0.1134 $m^2\ g^{-1}$, 0.2264 $m^2\ g^{-1}$, and 0.0015 $m^2\ g^{-1}$, respectively. Similarly, the total pore volumes for these mesh sizes were observed to be 3.0465×10^{-4} $cm^3\ g^{-1}$, 6.9283×10^{-4} $cm^3\ g^{-1}$, and 5.3337×10^{-4} $cm^3\ g^{-1}$, respectively. Additionally, the total pore diameters were 5.3 nm, 4.9 nm, and 1.5 nm for the MPH powder with mesh sizes of 90 μm, 120 μm, and 150 μm, respectively. Here, it was clearly observed that 120 μm MPH powder showed a larger surface area among all the compositions. Although 120 μm MPH powder has a smaller pore diameter than 90 μm MPH powder, it has a greater pore volume and surface area, which is possibly responsible for higher absorbency as discussed in a later section. Moreover, from the BJH pore size distribution curve, it was clearly noticed that the average pore diameter of the developed powder was between 1 and 5 nm which signifies micro- and mesopores according to the IUPAC definition. The 120 μm particle size exhibits a significantly larger surface area and major characteristics of pore size distribution within 4 nm demonstrating its potential significance for higher liquid absorbency and other desired properties. To the best of our knowledge, BET analysis has not yet been performed on MPH particles. Therefore, this MPH particle size was considered optimal for developing a modified formulation.

3.3. Free absorbency

Free absorbency test was carried out using variable mediums like distilled water, 0.9 wt% saline solution and sheep blood to evaluate the absorbency of the developed sample.

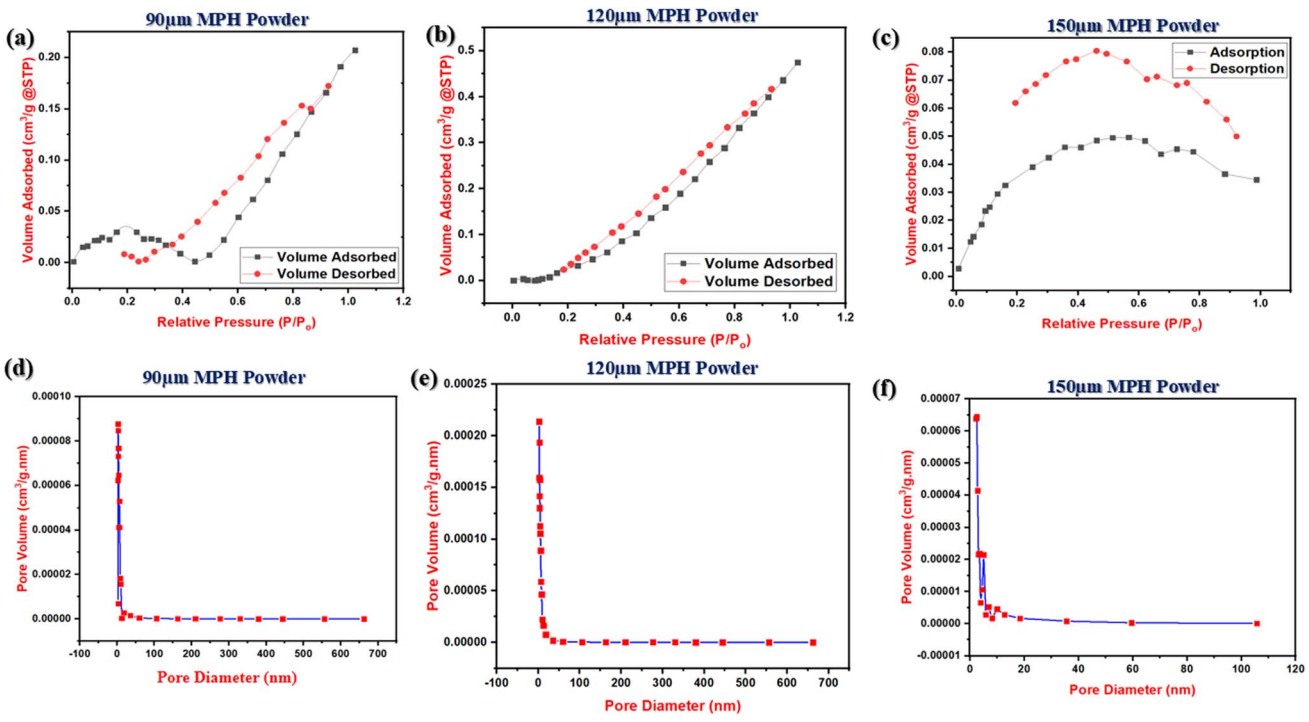

Fig. 2 (a–c) BET adsorption–desorption isotherms for 90 μm, 120 μm and 150 μm MPH powder respectively and (d–f) BJH pore size analysis of 90 μm, 120 μm and 150 μm MPH powder respectively.

Table 2 BET surface area and BJH pore size measurement for developed MPH powder of various sizes (mesh size) of 90–150 μm

No.	Sample code	Parameters	Results
1	90 μm MPH powder	BET surface area	0.1134 ± 0.05 $m^2 g^{-1}$
		Pore volume	0.00030465 ± 0.0006 $cm^3 g^{-1}$
		Pore diameter	5.39 ± 0.02 nm
2	120 μm MPH powder	BET surface area	0.2264 ± 0.03 $m^2 g^{-1}$
		Pore volume	0.00069283 ± 0.0007 $cm^3 g^{-1}$
		Pore diameter	4.98 ± 0.01 nm
3	150 μm MPH powder	BET surface area	0.0015 ± 0.04 $m^2 g^{-1}$
		Pore volume	0.00053337 ± 0.0003 $cm^3 g^{-1}$
		Pore diameter	1.56 ± 0.06 nm

3.3.1. Influence of CA concentration on absorbency in various mediums. Fig. 3 shows the influence of neat 5 wt% and 10 wt% cellulose acetate concentration on absorbency in various liquid mediums like distilled water and 0.9 wt% saline solution. Generally, CA accumulates more liquid immediately after immersion as it consists of hydroxyl groups within its composition which contributes to an increase in the final weight. As observed in Fig. 3(a) for immersion in distilled water, for a shorter time span of 10 s (0.166 min), the percentage of absorbency in 5 wt% and 10 wt% CA membrane was found to be 176.4% and 77.1% respectively, which further revealed the fact that neat 5 wt% CA membrane exhibited nearly 99.3% higher absorbency as compared with 10 wt% CA composition. A similar increased trend in absorbency value for 5 wt% CA was observed in distilled water after immersion for a period of 1 min, 5 min, 10 min, 15 min, and 30 min. Nevertheless, beyond 60 min in the case of 10 wt% CA membrane, an increased absorbency value along with some structural disintegration was observed. Furthermore, Fig. 3(b) shows the free absorbency of the neat 5 wt% CA and 10 wt% CA membranes in 0.9 wt% saline medium. Similar to that observed in distilled water medium, the overall absorbency performance was better for 5 wt% CA than for 10 wt% CA in saline solution which is possibly because structural integrity in the former membrane was maintained throughout the experiment. Additionally, the 5 wt% CA sample has a strongly crosslinked porous structure that maintains its structural integrity by storing more liquid within it. In comparison, at 0.166 min and 1 min, 5 wt% neat CA had immediate absorbency values of 75.39% and 85.19% higher than its 10 wt% CA counterpart. Immediate sorption without disintegration in structure is essential for our targeted application; thus 5 wt% CA was optimized and taken into consideration as a base material for the preparation of composite membranes.

3.3.2. Effect of incorporation of MPH powder within 5 wt% CA in various liquid mediums. Fig. 4 summarizes the comparison in liquid absorbency between the neat CA and the modified CA membranes encapsulated with MPH powder. As evident from the figure, 1 wt% MPH powder-loaded CA-modified membrane (MCA-2) showed maximum absorption among all the tested compositions. As shown in Fig. 4(a), after 10 min of distilled water immersion, MCA-2 showed 204.51% absorbency, which is approximately 105% greater than that of neat CA. It was also observed that MCA-2 showed absorbencies of approximately 279.6%, 320.9%, 390.1%, 399.6% and 407.6% at 30, 60, 180, 360 and 1440 min, respectively. Similarly, in saline medium, MCA-2 showed a 193.42% greater absorbency value than that of neat CA composition after 30 minutes of immersion. Throughout the test, MCA-2 justified its improved sorption performance in the saline medium due to the better

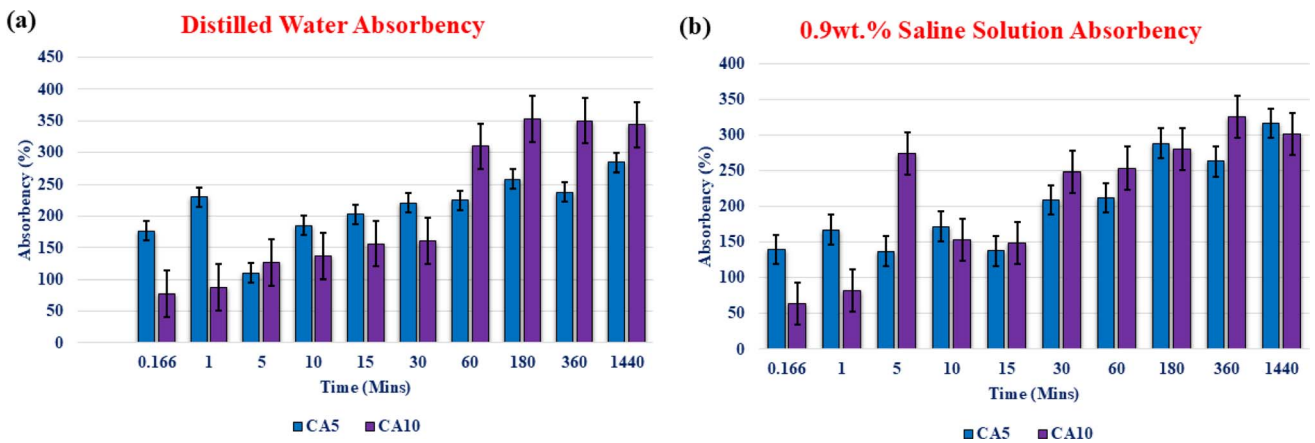

Fig. 3 Absorbency of neat cellulose acetate membrane samples at 5 wt% and 10 wt% in (a) distilled water and (b) 0.9 wt% saline solution.

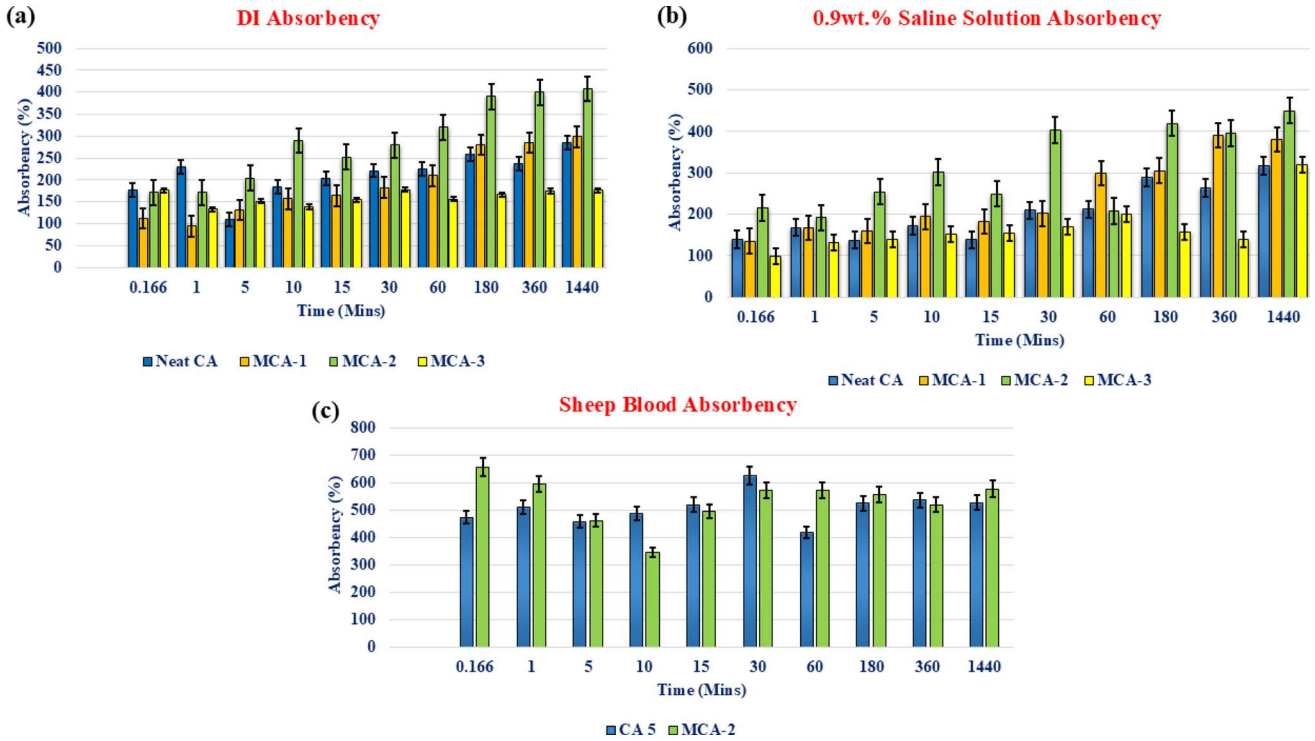

Fig. 4 Absorbency of neat CA, MCA-1, MCA-2, and MCA-3 membrane samples in (a) distilled water, (b) 0.9 wt% saline solution, and (c) sheep blood solution.

capillary action within it. The smaller particle size of MPH powder leads to an effective surface area of exposure and its microporous hollow channel structure is primarily responsible for efficient capillary action in the MCA-2 membrane which was chosen as the optimized formulation. Furthermore, Fig. 4(c) shows absorbency between neat CA and the optimized MCA-2 membrane through defibrinated sheep blood solution. For this test, defibrinated sheep blood with a marginally alkaline pH of 7.2–7.4 was taken as the replica of female body fluid because sheep blood contains a coagulation system that is closer to that of human body fluid (pH 7.4) than either pigs or dogs.[26,53] The test results revealed that MCA-2 can absorb 655.7% of blood at an immediate sorption time of 10 s Which is 182.9% greater than that of neat CA. Besides this, MCA-2 also showed a significant increase in absorbency throughout the experiment without any structural disintegration. Phase-inverted membranes absorb more blood because of the porous nature and enhanced roughness which is discussed in later sections. Furthermore, the crosslinked structure of the MPH powder and its greater liquid accumulation at a pH of approximately 7.2–7.4 allow the proper retention of sheep blood, resulting in an apparent increase in the absorption of the modified membrane. Thus, it was confirmed that the MCA-2 composition is the most appropriate formulation for use as an absorbent core material.

The significance of using the current approach for developing a fully biodegradable absorbent core for female hygiene applications is highlighted when compared to results reported for other absorbent materials. An absorbent material of carboxymethylcellulose crosslinked with epichlorohydrin reported by Alam *et al.*[54] showed an absorbency of 118 g g^{-1} in saline solution within 40 h, while our material showed immediate absorption characteristics within an hour, making it ideal for female hygiene products. In another study, cellulose acetate nanofibers were developed with a moderate absorption capacity of 19 g g^{-1}, but some structural disintegration occurred after some hours.[28,55] In contrast, the current developed material retained its structural integrity for 24 h. Additionally, research by Witono *et al.*[56] described cassava starch-based absorbent material grafted with polyacrylic acid which had a water absorbency of 63 g g^{-1}. However, the authors reported the use of a non-biodegradable material whereas the developed membrane sample is completely biodegradable. Thus, the MCA-2 composition signifies its suitability as an environmentally friendly absorbent core for female hygiene applications.

3.4. Absorbency under load (AUL test)

Fig. 5 compares the free absorbency and AUL of all the developed samples. The AUL test was carried out to measure the absorbency of the membrane under a certain applied load. It is evident that the MPH-loaded modified membranes showed greater absorbency at the given load than the free absorbency test at 60 min 1 wt% MPH-loaded membrane (MCA-2) showed an optimum absorbency of 439.69% under loading in the saline medium, which was 254.8% higher than that of the neat CA membrane. This result revealed that the presence of MPH having optimum surface area incorporated in the CA membrane greatly influences the absorbency performance,[51] which can be

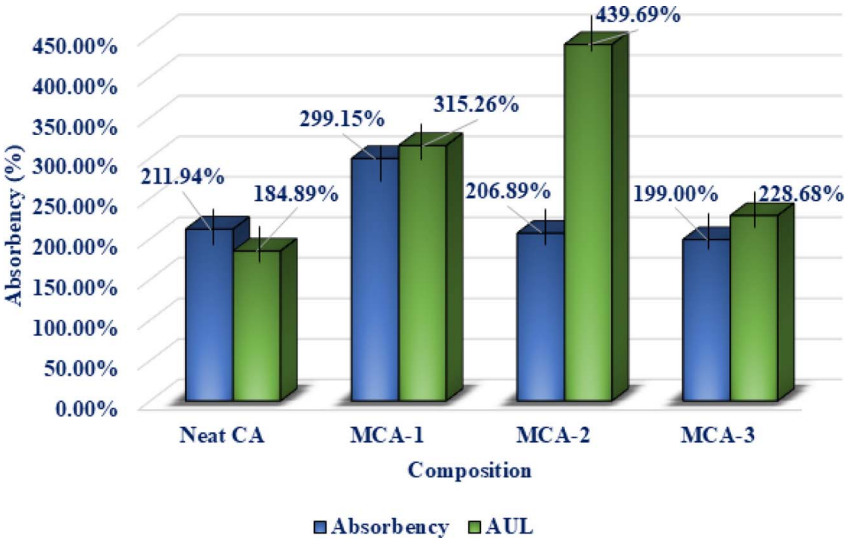

Fig. 5 A comparative study of free absorbency and absorbency under load at 60 min for neat CA and MCA-2 membrane samples.

due to similar facts of a more crosslinked structure that influences the capillary action in the membrane, thus contributing to greater absorbency under a specific load for a certain duration. Moreover, all the compositions exhibit apparently higher AUL values as compared to free absorbency due to the occurrence of consequential osmotic and ionic effects at applied compressive load.

3.5. XRD analysis

The characteristics of the crystalline or amorphous phase present in a sample can be easily determined by the structural position and peak intensity in XRD patterns. Fig. 6 shows the XRD patterns of *Mimosa pudica* seed, MPH powder, neat CA and MCA membrane samples. *Mimosa pudica* seeds as well as the powder prepared from the dried mucilage released from the seeds are semi-crystalline in nature, and the presence of subordinate hydrogen bonds decreases their crystallinity. As a result, a larger and broader hump could be seen at 2θ of approximately 22.15° in the diffraction pattern which reveals the lack of long-range order indicative of some amount of amorphous material. However, in the powder form, this peak intensity apparently decreased, suggesting an increase in the number of hydroxyl groups inside the powder, indicating an increase in amorphous nature. Patterns of both the CA and MCA samples exhibit a broader hump at approximately 8° and 22°, respectively, which established a clear amorphous structure within them.[57,58]

3.6. Morphological analysis

Fig. 7 displays SEM and FESEM micrographs of *Mimosa pudica* seeds and MPH powder. Fig. 7(a) shows the SEM micrograph of a channelled mucilage layer on the *Mimosa pudica* seed surface, while Fig. 7(b) depicts the three-dimensional, crosslinked,

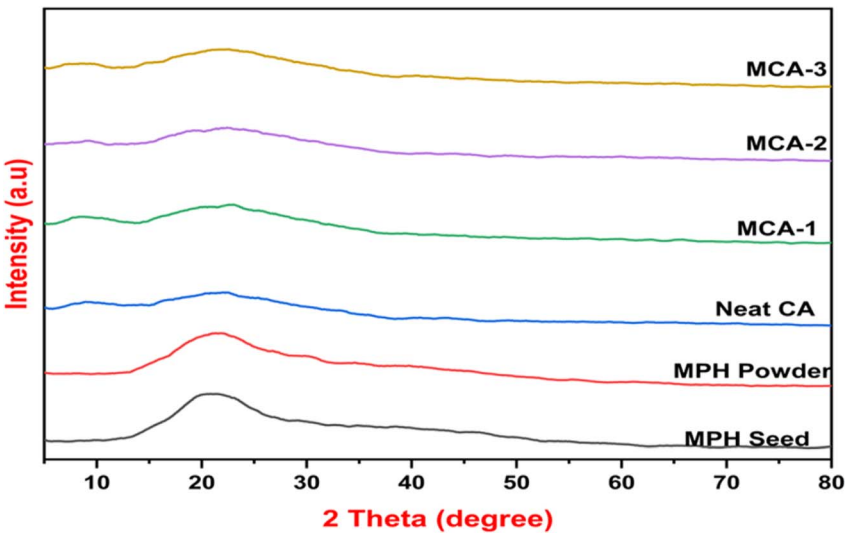

Fig. 6 XRD patterns of (i) *Mimosa pudica* seed, (ii) MPH powder, (iii) neat CA, (iv) MCA-1, (v) MCA-2, and (vi) MCA-3 samples.

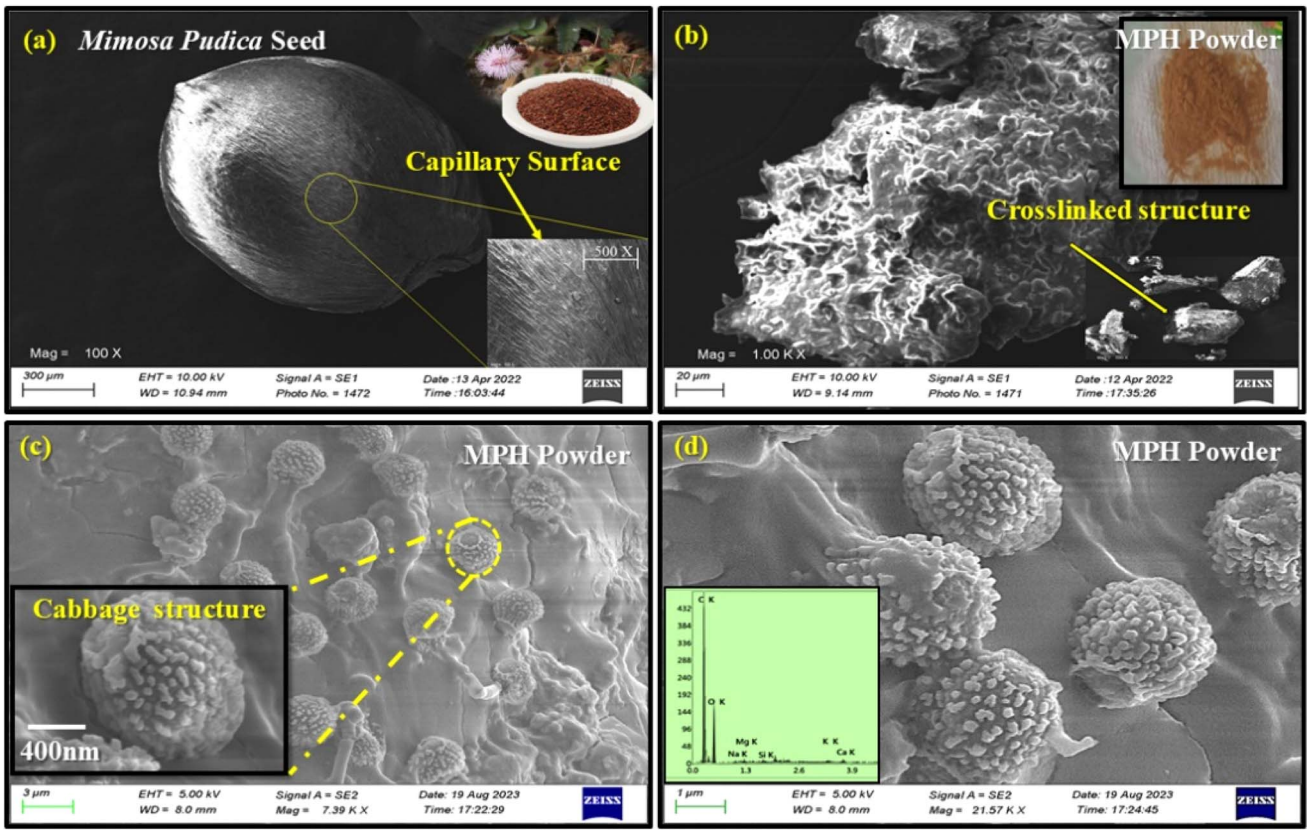

Fig. 7 SEM micrographs of (a) *Mimosa pudica* seed and (b) MPH powder. (c and d) FESEM micrographs with EDX analysis of MPH powder (quantitative analysis).

granular structure of the MPH powder. For more detailed visualization, the cabbage-like flower structure of the MPH powder was observed in the FESEM micrographs (Fig. 7(c and d)). These images reveal that the powder derived from the dried mucilage released from the seeds develops numerous hollow capillary channels and interconnected macropores, significantly enhancing its capacity for greater accumulation. The distinct three-dimensional crosslinked, granular structure seen in Fig. 7(c and d) is primarily responsible for the increased liquid absorbency.[59,60] Energy dispersive X-ray (EDX) analysis of the MPH powder, detailed in Table 3, revealed various major elements including carbon, oxygen, sodium, magnesium, silicon, potassium and calcium present in the developed powder. Primarily, carbon (C) and oxygen (O) are mainly responsible for the liquid absorption process. Fig. 8 shows the surface morphology of the developed membranes, whereas Fig. 9 presents their EDX analysis. The neat CA membrane (Fig. 8(a)) exhibits a porous structure throughout its surface indicating the presence of hydroxyl groups within its composition. After the incorporation of MPH into the polymeric matrix, the porosity increased significantly, as shown in Fig. 8(b–d). In MCA-2, 1 wt% MPH loaded to the CA matrix led to a homogenous dispersion and a miscible porous matrix–filler interface with numerous capillary channels (Fig. 8(c)), manifesting a higher liquid absorbency through various liquid mediums. Additionally, this uniform dispersion and interconnected porous structure also enhance other characteristic properties, which will be discussed in a later section. However, the FESEM micrographs of the 2 wt% loaded modified membrane sample (MCA-3) shows reduced miscibility and some granular structure, indicating that excessive MPH concentration may lead to agglomeration, which leads to a reduction in absorbency performance. Elemental quantitative analysis *via* EDX, presented in Fig. 9, revealed the predominance of carbon and oxygen, with their constituent percentages significantly contributing to the liquid absorption properties of the MPH-loaded CA membrane. The carbon and oxygen in the cellulose acetate membrane contribute to its porous structure, supporting the formation of hydroxyl and ester groups. These groups facilitate hydrogen bonds with various liquid mediums,

Table 3 EDX results of developed MPH powder

Element	Weight (%)	Atomic (%)
C K	71.0	77.0
O K	27.5	22.3
Na K	0.3	0.2
Mg K	0.4	0.2
Si K	0.2	0.1
K K	0.3	0.1
Ca K	0.4	0.1

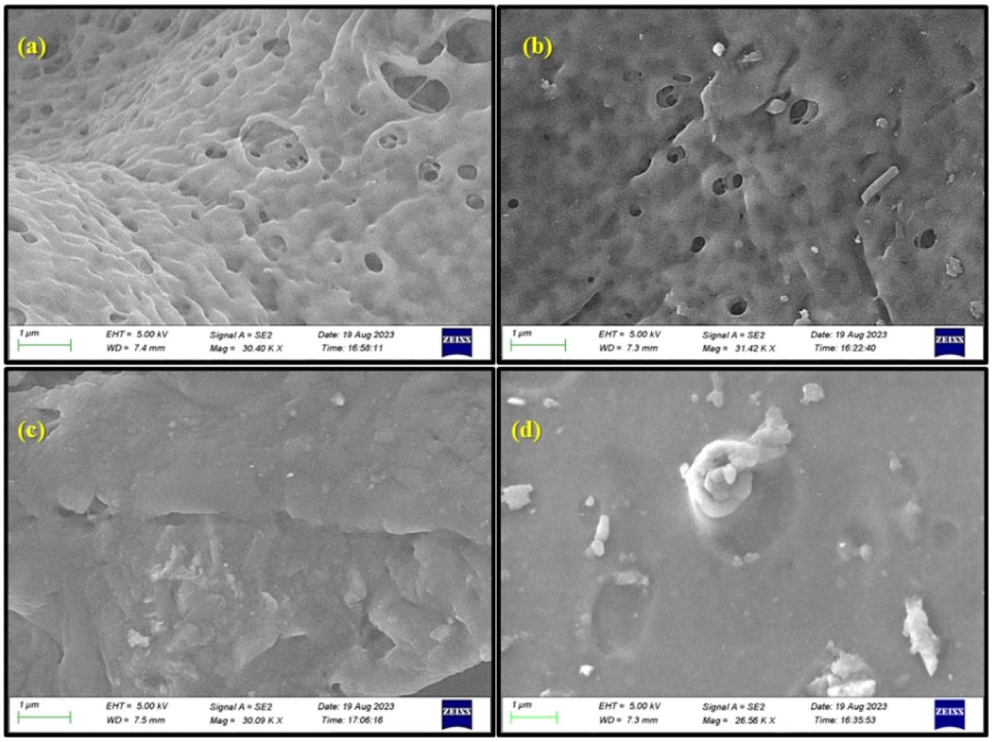

Fig. 8 FESEM micrographs of (a) neat CA, (b) MCA-1, (c) MCA-2 and (d) MCA-3.

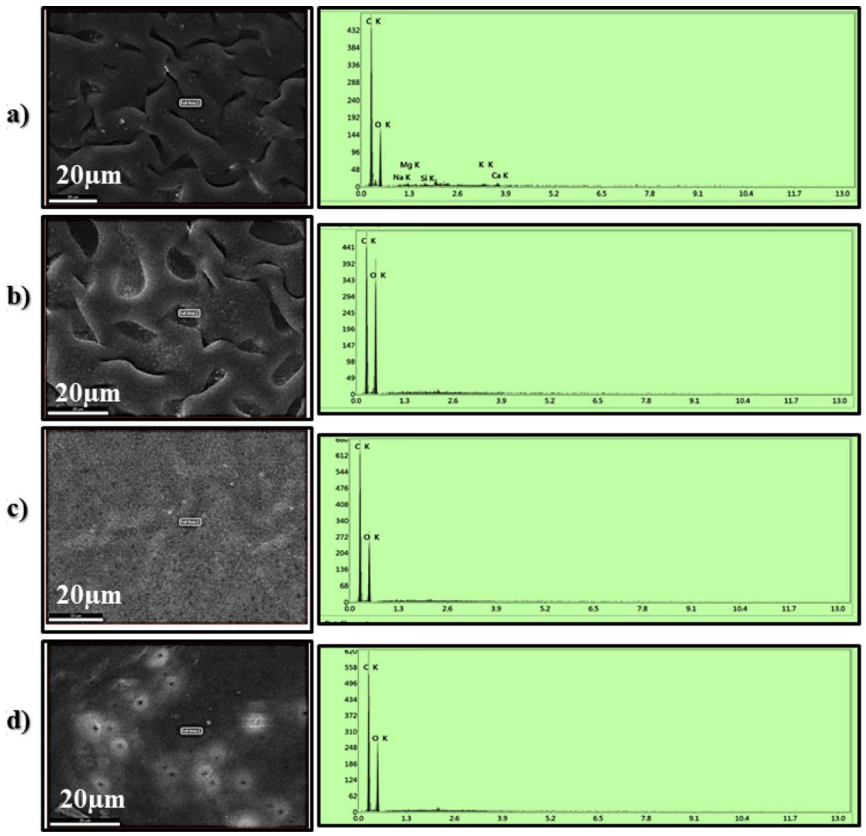

Element	Weight (%)	Atomic (%)
C K	62.5	68.9
O K	37.5	31.1

Element	Weight (%)	Atomic (%)
C K	60.7	67.3
O K	39.3	32.7

Element	Weight (%)	Atomic (%)
C K	69.6	75.3
O K	30.4	24.7

Element	Weight (%)	Atomic (%)
C K	68.3	74.2
O K	31.7	25.8

Fig. 9 FESEM images with EDX analysis of (a) neat 5 wt% CA, (b) MCA-1, (c) MCA-2 and (d) MCA-3.

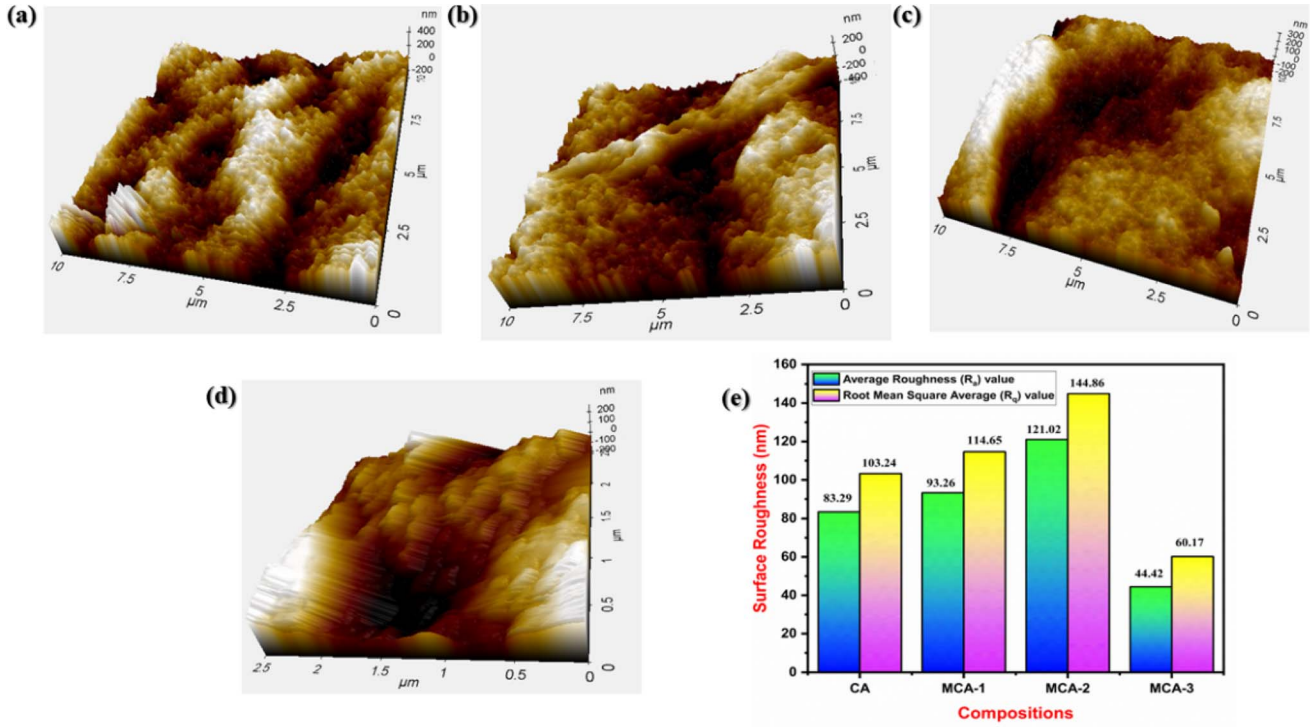

Fig. 10 AFM 3D images of (a) neat 5 wt% CA, (b) MCA-1, (c) MCA-2 and (d) MCA-3. (e) Graphical representation of average roughness (R_a) and root mean square roughness (R_q).

enhancing the hydrophilic properties of the developed membrane and enabling it to accumulate more liquid within it.

3.7. Topographical analysis

The surface topography of the developed membranes was analysed through AFM in noncontact mode, as shown in Fig. 10. The surface roughness increased after incorporation of the MPH powder, as clearly visible in the three-dimensional structure of the samples. Neat CA exhibited relatively less roughness, whereas MCA-2 showed the maximum roughness on the surface.[58] Furthermore, the surface roughness parameters R_q (square average roughness) and R_a (arithmetic mean roughness) for all the samples were calculated by AFM analysis software and are presented in Fig. 10(e). When comparing modified samples to neat CA, the R_a and R_q values significantly increased for MCA-2, indicating that the increase in surface roughness was influenced by the presence of the MPH filler. Thus, a higher surface roughness is preferable for fluid absorbency, and as a whole, these results corroborate the findings of FESEM analysis.

3.8. Mechanical analysis

Fig. 11(a) depicts tensile stress–strain curves for all the developed samples. As observed from the figure, neat CA shows a tensile strength of 1.29 ± 0.4 MPa with an elongation of 3.23%. Incorporation of MPH within the CA in the case of MCA-1, MCA-2, and MCA-3 showed an increase of tensile strength to 2.06 ± 0.5, 2.45 ± 0.2 and 1.20 ± 0.6 MPa respectively. MCA-2 showed the maximum value among all the compositions that can enable the membrane to withstand an applied load of 6.31 N with an elongation of 13.67%. This improvement in mechanical properties has been corroborated from the FESEM micrographs shown in Fig. 8, which reveal a uniform and interconnected crosslinked porous structure with well-dispersed MPH particles within the polymer matrix. This structure enhances stress distribution and strengthens the membrane's ability to withstand an applied tensile stress. However, an increase in MPH concentration in MCA-3 possibly resulted in agglomeration of the filler thereby resulting in a decrease in the tensile strength. Besides this, CA exhibits only an elastic region without or with minimal amount of plastic regime, whereas MCA-1 and MCA-2 showed resistance against the applied load thereby depicting a higher modulus value. In the case of neat CA, tensile stress increased abruptly with increased strain and revealed typical characteristics of a brittle material. Similarly, in the case of MCA-3, the characteristics of the peak revealed a typical case of a brittle material which is due to similar facts of agglomeration of MPH powder within the neat CA matrix as corroborated from the FESEM micrographs shown in Fig. 8. However, in the case of MCA-1 and MCA-2, the stress–strain curves showed an increase in strain with an application of stress exhibiting the ductile characteristics with a higher elongation of 20.03% and 13.67% respectively. The modulus values for MCA-1, MCA-2 and MCA-3 are 77.19 ± 0.4 MPa, 120.66 ± 0.5 MPa and 52.31 ± 0.3 MPa respectively as shown in Fig. 11(b). Here, MCA-2 showed approximately 91.25 MPa higher value as compared to the neat CA sample. All the mechanical parameters are listed in Table 4. From the mechanical findings, MCA-2 is considered as the optimized

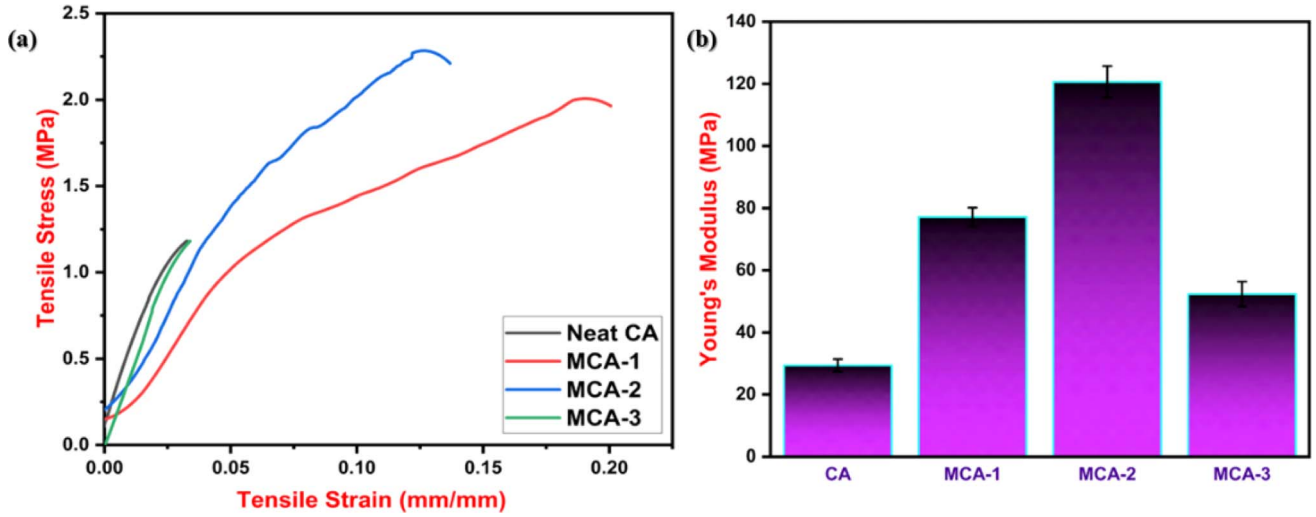

Fig. 11 (a) Tensile stress–tensile strain curves of (i) neat 5 wt% CA, (ii) MCA-1, (iii) MCA-2 and (iv) MCA-3. (b) Young's modulus value for all the compositions.

Table 4 Mechanical properties of neat CA and MCA membranes

No.	Sample code	Tensile strength (MPa)	Elongation (%)
1	Neat CA	1.29 ± 0.4	3.23 ± 0.4
2	MCA-1	2.06 ± 0.5	20.03 ± 0.6
3	MCA-2	2.45 ± 0.2	13.67 ± 0.5
4	MCA-3	1.20 ± 0.6	3.37 ± 0.6

formulation for further characterization and analysis as an absorbent core.

3.9. Thermal analysis

Fig. 12(a) and (c) show the thermal degradation behaviour of *Mimosa pudica* seed, MPH powder (90–150 μm) and MCA membrane samples, whereas Fig. 12(b and d) displays their derivative thermograms for all the developed samples. As observed from the thermograms, two-step degradation was visualised for *Mimosa pudica* seed and various-sized MPH powder. The first degradation was noticed at 25–100 °C due to the hydroxyl groups or moisture content in the MPH, whereas the second degradation occurred up to 480 °C for approximately 81% decomposition of the glucuronoxylan compound present in the MPH powder. The 120 μm MPH powder size exhibited the lowest ash content of 2.81% among all powder samples. Further, Fig. 12(c) shows the three steps of degradation for neat CA and MCA membrane samples. For a neat CA sample, the first weight loss was visualized in a range of 25–120 °C because of the evaporation of moisture or loss of hydroxyl groups present in the CA. Meanwhile, a significant degradation of 87.72% was noticed within the temperature range of 300–400 °C due to the degradation of the polymeric backbone or breakdown of polysaccharide compounds. The final weight loss is attributed to the remaining ash content produced from the overall degradation. Besides this, a similar trend was followed in the MCA samples; however, a plateau was clearly visualized for them at a temperature of 280–320 °C with maximum degradation behaviour. Further, there was negligible ash content noticed for the MCA composition suggesting the complete depolymerization of the polymer. $T_{50\%}$ for neat CA, MCA-1, MCA-2, and MCA-3 were approximately 365 °C, 402 °C, 430 °C, and 426 °C respectively, which were clearly observed from the DTG thermograms which revealed improved thermal stability of CA in the MCA-2 membrane possibly due to the formation of a crosslinked network in the latter in the presence of MPH powder. All the thermal parameters are tabulated in Table 5.

3.10. Antibacterial analysis

The antibacterial efficiency of the material used in the absorbent core provides additional protection for the safe use of sanitary napkins. Fig. 13 shows the results of the antibacterial analysis of the developed membranes by the disc diffusion method. After 24 h of incubation, the antibacterial agents of the developed formulation diffused to the agar media and inhibited the growth of the test microorganisms. The inhibition zones against *Escherichia coli* (*E. coli*: Gram negative) and *Staphylococcus aureus* (*S. aureus*: Gram positive) pathogenic bacteria were measured in mm to assess the antibacterial activity of the developed formulations. From the results, as shown in Fig. 13, it was observed that neat cellulose acetate exhibited a minimal inhibition zone which could not be measured; in contrast, MCA-2 had a clear inhibition zone. Six-month-old MCA-2 samples also exhibited antibacterial activity, as indicated by the longevity or lifespan of these samples. The test was performed thrice for complete proper property evaluation, and it was observed that the modified formulation showed a greater inhibition zone against *E. coli* bacteria. The presence of phytochemicals and natural antioxidant compounds such as flavonoids, terpenoids, coumarins, alkaloids and saponins is responsible for the improved antibacterial properties of the MPH powder formulation,[33–35] and the modified formulation

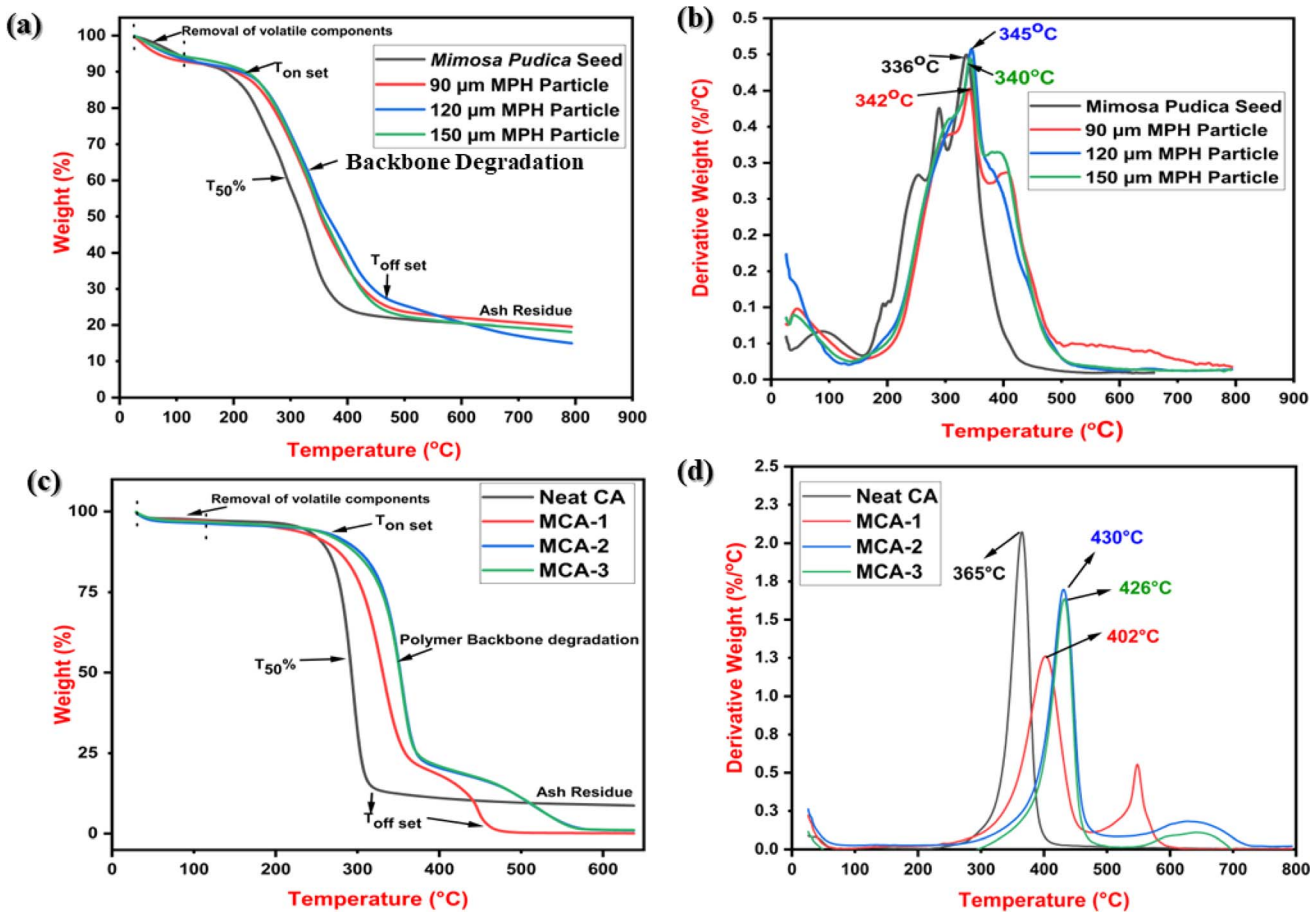

Fig. 12 (a) TGA thermograms for *Mimosa pudica* seed and 90–120 µm MPH powder. (b) Derivative thermograms (DTG). (c) TGA thermograms of (i) neat CA, (ii) MCA-1, (iii) MCA-2, (iv) MCA-3 and (d) DTG curves.

Table 5 TGA parameters of *Mimosa pudica* seed, MPH powder (particle size: 90–150 µm), CA and MCA membrane samples

No.	Sample code	Decomposition temperatures (°C)			Residue (%) at 600 °C
		T_{min}	$T_{50\%}$	T_{max}	
1	*Mimosa pudica* seed	103	336	404	3.12
2	90 µm MPH particle	80	342	396	6.34
3	120 µm MPH particle	85	345	408	2.69
4	150 µm MPH particle	90	340	389	3.15
5	Neat CA			368	8.77
6	MCA-1	115	402	447	0.92
7	MCA-2	120	430	528	0.67
8	MCA-3	120	426	536	1.07

(MCA-2) may be a potential candidate biobased absorbent core for use in sanitary napkins.

3.11. Soil burial test, ecotoxicity test and identification of bacteria through 16s rRNA sequencing

In the current scenario, disposal of menstrual hygiene products has been a matter of major concern as these synthetic polyacrylate-based products take nearly 500–700 years to completely degrade. The microorganisms present in the soil cannot digest and break the complex structured compounds, while they remain in the soil after degradation. In this context, a soil burial test (ASTM G160-12) was performed to evaluate the biodegradability of the developed sample at end of its service life. Here, the percentage weight loss of the membrane sample could not be measured due to the excess amount of water absorbed by the material during the test. Thus, only morphological inspection of the degraded samples was conducted after soil burial for time periods of 60, 120, and 180 days as shown in Fig. 14. Our developed product showed remarkable changes such as cracks and pores on the surface of the sample. MCA-2 membrane exhibited a higher degradation which is primarily due to the presence of MPH bio filler in the sample.[51] The hydroxyl, phenolic, and glucuronoxylan groups present in MPH contributed to favourable growth of the microorganisms that resulted in significant degradation.[61–63] Additionally, a degradation test of a commercial sample was undertaken as a control, in which negligible microbial growth along with some residues was observed (ESI 1†). CHN analysis of soil and the isolation of microorganisms using 16S rRNA sequencing were performed as shown in Fig. 15.

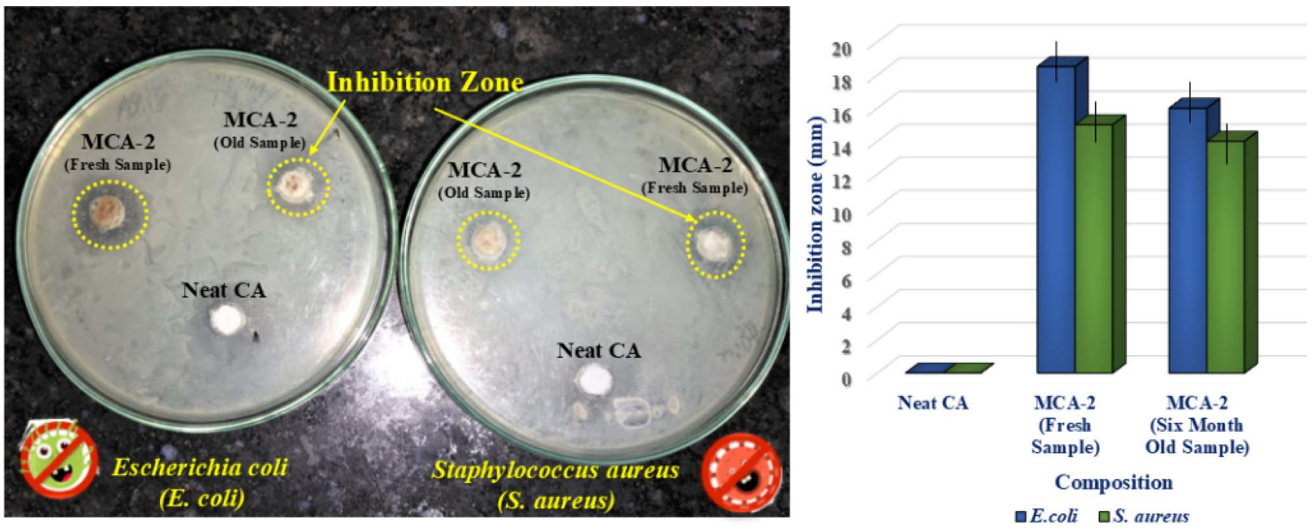

Fig. 13 Antibacterial activity analysis test of developed neat CA membrane and MCA-2 membrane samples against *Escherichia coli* and *Staphylococcus aureus* bacteria using the disc diffusion method.

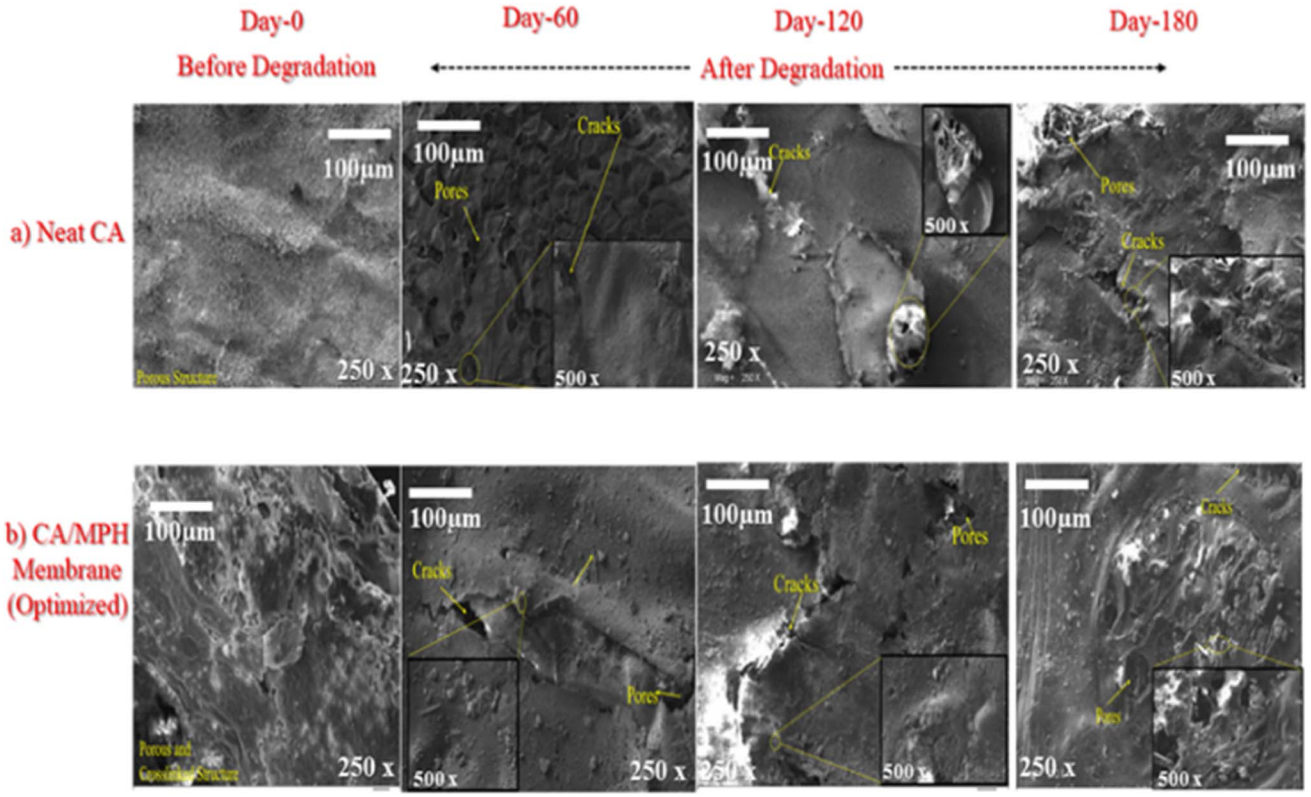

Fig. 14 SEM images of samples (before and after degradation): (a) neat CA; (b) MCA-2.

As observed in the CHN analysis of the soil, the elemental percentages of carbon, hydrogen, and nitrogen were 1.226%, 0.760%, and 0.097% for neat CA, and 1.949%, 0.516%, and 0.151% for MCA-2 samples, respectively. Besides this, while performing the soil burial test, an ecotoxicity test was also performed using Moong seed according to OECD guidelines and it was observed that there is no side effect in plant growth for our developed composition whereas some decreased amount of plant growth was visualized in the commercial sample degraded in soil. This clearly indicated its friendly impact on the environment. Moreover, the collected soil from the sample surface was examined and subjected to DNA genomic isolation according to the respective bacteria that caused degradation. Then ribosomal RNA (rRNA) sequencing

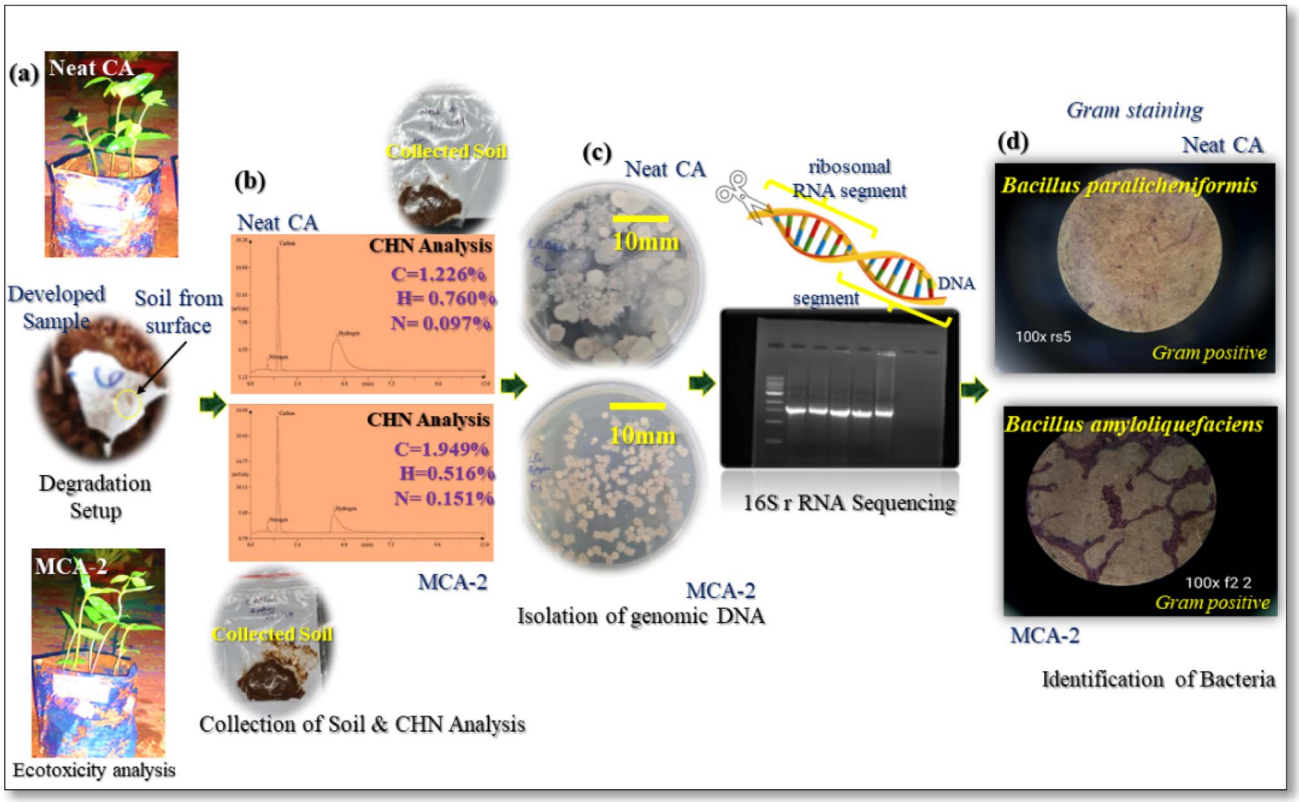

Fig. 15 (a) Ecotoxicity analysis, (b) CHN analysis of neat CA and MCA-2, (c) isolation of genomic DNA, and (d) Gram staining: identification of manifested bacteria responsible for degradation.

was performed to identify the specific sequence. From the microscopic images, as shown in Fig. 15(d), it was confirmed that the phyla of *Bacillus paralicheniformis* and *Bacillus amyloliquefaciens* might be affiliated with the majority of the 16S rRNA genomic sequence that exhibited a relative abundance exceeding 95% in the neat CA and MCA-2 formulation respectively. These two bacterial species are mainly Gram-positive bacterial species with versatile metabolic capabilities to degrade the complex polysaccharide structure very easily. These bacteria possess esterase and are involved in the enzymatic action for which easy cleavage of complex ester bonding associated with acetate group into smaller molecules and metabolism are possible. Additionally, in the MCA-2 sample, a supplemental pathway including esterase, cellulase and many other enzymes may be possible while enzymatic pathways degrade this composition effortlessly.[64–68] During this degradation process, plant growth in the soil can be possible without showing any side effects while growing. An additional study for the commercial sample was performed for better understanding as shown in ESI 1.† Overall, a complete glimpse of the decomposition pattern for the modified composition has been studied for the targeted application.

3.12. Mold growth resistance analysis

The commercial absorbent reference material showed an increase in mold patches after 10 days of exposure to 100% RH, as shown in ESI 1.† The mold growth in the commercial samples rapidly increased daily, whereas there was no visible mold growth in either the neat CA or MCA-2 samples until 20 days of exposure to moisture. On day 20, some patches in some samples of MCA-2 were visible in less quantity than those in neat CA, and on day 30, no notable growth was observed in MCA-2. This result revealed that the acrylic content in the cotton fibers of the commercial sample can quickly absorb moisture in large quantities. Besides this, some favourable conditions arise for fungal growth in commercial samples, which is not possible in MCA-2. MPH-filled CA membrane inhibited mold growth and interrupted regular mass transport through the bacterial cell wall because of its antibacterial properties. Furthermore, it can be sustained under high relative humidity conditions, resulting in slower mold growth even after 20 days of exposure to moisture. The commercial sample was able to absorb moisture from the saturated environment, and weight changes were observed, which were negligible for both neat CA and MCA-2.

4. Conclusions

MPH-based CA membrane was successfully developed using the NIPS method. Several characterization tests and property analyses were performed to investigate its overall performance. From the overall study, it was clearly observed that among all compositions, the CA membrane with 1% MPH additive (MCA-2) showed the maximum absorbency with values of 276.66%,

402.87%, and 572.5% in distilled water, 0.9 wt% saline solution and defibrinated sheep blood mediums respectively after 30 minutes of exposure in the respective mediums. It also exhibited the highest absorbency under load value of 439.69% in saline medium while maintaining its structural integrity. From the BET analysis, it was observed that incorporation of 120 μm MPH powder having a larger surface area, within the CA membrane, results in instantaneous liquid absorption. The presence of an amorphous structure of MPH powder was confirmed from the XRD patterns, while the FESEM micrographs revealed a cabbage crosslinked structure. Furthermore, the surface roughness parameters confirmed from the AFM analysis provide strong supplemental evidence for better absorbency in the MCA-2 sample than that of the neat CA membrane. The mechanical findings revealed a tensile load of 6.31 N and modulus of 120 ± 0.5 MPa with an elongation of 13.67 ± 0.2%. The developed MCA-2 membrane exhibits notable thermal and mold resistance properties, along with an efficient antibacterial property against *E. coli* and *S. aureus* bacteria. The soil burial test showed a decomposition pattern and 16S rRNA sequencing showed that *Bacillus amyloliquefaciens* bacteria might be responsible for decomposition of the membrane which was confirmed by the BLAST gene bank database. The studies concluded that the MCA-2 membrane has the desired attributes for use as an absorbent core in female hygiene products.

Data availability

All the data have been included in the main paper and additional data have been uploaded as part of ESI.†

Author contributions

Conceptualization, methodology, validation, investigation: Roshni Pattanayak, Sukanya Pradhan, Smita Mohanty; writing original draft: Roshni Pattanayak; writing – review & editing: Sukanya Pradhan and Smita Mohanty; supervision: Smita Mohanty.

Conflicts of interest

There are no conflicts to declare. However, some parts of this research have been included in our filed Indian patent with application number: 202231061640 (D.O.F. 28.10.2022 & Publication date 4.11.2022).

Acknowledgements

R. Pattanayak would like to acknowledge the Department of Science and Technology, Government of India (DST), for providing the Inspire fellowship (DST/INSPIRE Fellowship/2020/IF200480) and the authors would also like to thank the Centre of Excellence (CoE) on 'Manufacturing of Next Generation Bio-Medical Devices' from DCPC Govt. of India (F. No. 25012/01/2020-PC-II (FTS:16020)). The authors also would like to thank Ms Pranjal Mohanty, an M. Sc. Tech student from CIPET for her help during the powder synthesis process and also are grateful to Dr Debasmita Mohanty, Research associate, Mr Bhagaban Das, lab assistant, Mr Tusharkanta Nayak, Project Associate-I, and Ms Tapaswini Jena, scientific assistant for their kind help during the experimental methods. Special gratitude to Dr Shaikh Nausad Hossain, from Regional Institute of Biotechnology for the smooth conduct of all biological tests.

References

1 S. Sheikh, Where Does India Stand In Menstrual Hygiene Management?, Youth Ki Awaaz, 2020, Accessed: Mar. 27, 2023, https://www.youthkiawaaz.com/2020/11/state-of-mhm-a-look-into-government-policies/.

2 C. Kambala, A. Chinangwa, E. Chipeta, B. Torondel and T. Morse, Acceptability of menstrual products interventions for menstrual hygiene management among women and girls in Malawi, *Reprod. Health*, 2020, **17**(1), 185, DOI: 10.1186/S12978-020-01045-Z.

3 S. K. Kumar, Is your sanitary napkin safe?, The new indian express, 2013, Accessed: Jan 17, 2023, https://www.google.com/search?q=is+your+sanitary+napkin+safe%2C+the+new+indian+express&oq=is+your+sanitary+napkin+safe%2C+the+new+indian+express&aqs=chrome.0.69i59.7673j0j7&sourceid=chrome&ie=UTF-8.

4 J. H. Shin and Y. G. Ahn, Analysis of Polychlorinated Dibenzo-*p*-dioxins and Dibenzo-furans in Sanitary Products of Women, *Text. Res. J.*, 2007, **77**(8), 597–603, DOI: 10.1177/0040517507078786.

5 Y. S. Kwon, S. G. Choi, S. M. Lee, J. H. Kim, S. G. Kim, D. Y. Lee and J. S. Soe, Improved method for the determination of polychlorinated dibenzo-*p*-dioxins and dibenzofurans (PCDD/FS) in sanitary napkins, *Anal. Lett.*, 2020, **53**(2), 273–289, DOI: 10.1080/00032719.2019.1647226.

6 G. Bhor and S. Ponkshe, A Decentralized and Sustainable Solution to the Problems of Dumping Menstrual Waste into Landfills and Related Health Hazards in India, *Eur. J. Sustain. Dev.*, 2018, **7**(3), 334, DOI: 10.14207/ejsd.2018.v7n3p334.

7 S. Ishii, R. Katagiri, T. Kataoka, M. Wada, S. Imai and K. Yamasaki, Risk assessment study of dioxins in sanitary napkins produced in Japan, *Regul. Toxicol. Pharmacol.*, 2014, **70**, 357–362, DOI: 10.1016/j.yrtph.2014.07.020.

8 R. Borooah, H. N. Chanakya, S. Dasappa, "Investigations into the performance of single chamber sanitary napkin incinerators with emphasis on CO and CO_2 emissions," *W. Management*, Elsevier, vol. 102, 2020, pp. 667–676, doi: DOI: 10.1016/j.wasman.2019.11.032.

9 M. He, Y. Zhao, J. Duan, Z. Wang, Y. Chen and L. Zhang, Fast contact of solid-liquid interface created high strength multi-layered cellulose hydrogels with controllable size, *ACS Appl. Mater. Interfaces*, 2014, **6**(3), 1872–1878, DOI: 10.1021/am404855q.

10 J. Ma, X. Li and Y. Bao, Advances in cellulose-based superabsorbent hydrogels, *RSC Adv.*, 2015, **5**(73), 59745–59757, DOI: 10.1039/C5RA08522E.

11 S. Ahmad, M. Ahmad, K. Manzoor, R. Purwar and S. Ikram, A review on latest innovations in natural gums based hydrogels: Preparations & applications, *Int. J. Biol. Macromol.*, 2019, **136**, 870–890, DOI: 10.1016/J.IJBIOMAC.2019.06.113.

12 C. L. Luchese, J. B. Engel, and I. C. Tessaro, "Disposable, reusable and biodegradable hygiene products," *Antimicrobial Textiles from Natural Resources*, 2021, pp. 421–454, doi: DOI: 10.1016/B978-0-12-821485-5.00003-2.

13 M. R. M. Abed, S. C. Kumbharkar, A. M. Groth, K. Li, "Ultrafiltration PVDF Hollow Fibre Membranes with Interconnected Bicontinuous Structures Produced *via* a Single-step Phase Inversion Technique," *JMS*, Elsevier, vol. 407–408, 2012, pp. 145–154, doi: DOI: 10.1016/j.memsci.2012.03.029.

14 G. Akay, B. Dissanayake and A. Morgan, Process Intensification in Particle Technology: Production of Powder Coatings by Nonisothermal Flow-Induced Phase Inversion, *Ind. Eng. Chem. Res.*, 2011, **50**(6), 3239–3246, DOI: 10.1021/IE101516R.

15 R. R. S. Thakur, H. L. McMillan and D. S. Jones, Solvent induced phase inversion-based *in situ* forming controlled release drug delivery implants, *J. Controlled Release*, 2014, **176**(1), 8–23, DOI: 10.1016/J.JCONREL.2013.12.020.

16 A. R. C. Duarte, J. F. Mano and R. L. Reis, Dexamethasone-loaded scaffolds prepared by supercritical-assisted phase inversion, *Acta Biomater.*, 2009, **5**(6), 2054–2062, DOI: 10.1016/J.ACTBIO.2009.01.047.

17 D. J. Miller, T. Henning and W. Grünbein, Phase inversion of W/O emulsions by adding hydrophilic surfactant — a technique for making cosmetics products, *Colloids Surf., A*, 2001, **183–185**, 681–688, DOI: 10.1016/S0927-7757(01)00494-0.

18 C. V. Goethem, D. de Beeck, A. Ilyas, M. Thijs, G. Koeckelberghs, P. E. M. Aerts and I. F. J. Vankelecom, Ultra-thin and highly porous PVDF-filters prepared *via* phase inversion for potential medical (COVID-19) and industrial use, *J. Membr. Sci.*, 2021, **639**, 119710, DOI: 10.1016/j.memsci.2021.119710.

19 S. L. Duraikkannu, R. Castro-Muñoz and A. Figoli, A review on phase-inversion technique-based polymer microsphere fabrication, *Colloids Interface Sci. Commun*, 2021, **40**, DOI: 10.1016/J.COLCOM.2020.100329100329.

20 Y. Tang, Y. Lin, D. M. Ford, Q. Xianghong, M. R. Cervellere, P. C. Millett and X. Wang, A review on models and simulations of membrane formation *via* phase inversion processes, *J. Membr. Sci.*, 2021, **640**, 119810, DOI: 10.1016/J.MEMSCI.2021.119810.

21 G. Reshma, C. R. Reshmi, S. V. Nair and D. Menon, Superabsorbent sodium carboxymethyl cellulose membranes based on a new cross-linker combination for female sanitary napkin applications, *Carbohydr. Polym.*, 2020, **248**, 116763, DOI: 10.1016/J.CARBPOL.2020.116763.

22 N. Ghadyalpatil, "Sanitary Pads Can Cause Cancer – Reasons and Prevention.", Times of India, 2023, Accessed: Dec. 18, 2023. Available: https://timesofindia.indiatimes.com/blogs/voices/sanitary-pads-can-cause-cancer-reasons-and-prevention/.

23 C. J. Gao, F. Wang, H. M. Shen, K. Kannan and Y. Guo, Feminine Hygiene Products - A Neglected Source of Phthalate Exposure in Women, *Environ. Sci. Technol.*, 2020, **54**(2), 930–937, DOI: 10.1021/ACS.EST.9B03927.

24 J. Ma, X. Li and Y. Bao, Advances in cellulose-based superabsorbent hydrogels, *RSC Adv.*, 2015, **5**(73), 59745–59757, DOI: 10.1039/C5RA08522E.

25 S. Bhaladhare and D. Das, Cellulose: a fascinating biopolymer for hydrogel synthesis, *J. Mater. Chem. B*, 2022, **10**(12), 1923–1945, DOI: 10.1039/D1TB02848K.

26 O. Azhar, Z. Jahan, F. Sher, M. B. K. Niazi, S. J. Kakar and M. Shahid, Cellulose acetate-polyvinyl alcohol blend hemodialysis membranes integrated with dialysis performance and high biocompatibility, *Mater. Sci. Eng., C*, 2021, **126**, 112127, DOI: 10.1016/j.msec.2021.112127.

27 T. Sudiarti, D. Wahyuningrum, B. Bundjali and I. Made Arcana, Mechanical strength and ionic conductivity of polymer electrolyte membranes prepared from cellulose acetate-lithium perchlorate, *IOP Conf. Ser.: Mater. Sci. Eng.*, 2017, **223**(1), 012052, DOI: 10.1088/1757-899X/223/1/012052.

28 S. Yadav, M. P. Illa, T. Rastogi and C. S. Sharma, High absorbency cellulose acetate electrospun nanofibers for feminine hygiene application, *Appl. Mater. Today*, 2016, **4**, 62–70, DOI: 10.1016/J.APMT.2016.07.002.

29 J. Wolfs and M. A. R. Meier, A more sustainable synthesis approach for cellulose acetate using the DBU/CO_2 switchable solvent system, *Green Chem.*, 2021, **23**, 4410–4420, DOI: 10.1039/D1GC01508G.

30 E. A. Parray, M. U. Rehman, M. U. D. Khanday, T. Bhat, M. T. Ali, M. A. Wani, M. A. Hajam, M. T. Ali, T. Islam and S. Mehraj, Drought management strategies in fruit crops: Anoverview, *J. Pharmacogn. Phytochem.*, 2017, **6**(6), 2423–2425, Available online: https://www.phytojournal.com/.

31 L. M. Hernandez, O. D. Rubio, A. C. Garcia and J. M. Aguilera, Mucilage from Chia Seeds (Salvia hispanica) Microestructure, Physico-Chemical Characterization and Applications in Food Industry, Phd thesis, academia.edu, 2012, https://www.academia.edu/8381315/.

32 R. Pattanayak, T. Jena, S. Pradhan and S. Mohanty, Recent advancement of bio-based super absorbent polymer and its biodegradable and recycling behavior: a vision and future, *Polym-Plast Tech Mat.Polymer-Plastics Technology and Materials*, 2023, **62**(10), 1290–1317, DOI: 10.1080/25740881.2023.2204982.

33 R. Lakshmibai and D. Amirtham, Antimicrobial Activity Of Mimosa Pudica Thorns, *Int. Res. J. Pharm.*, 2018, **9**(6), 202–206, DOI: 10.7897/2230-8407.096117.

34 V. A. Niraimathee, V. Subha, R. S. E. Ravindran and S. Renganathan, Green synthesis of iron oxide nanoparticles from Mimosa pudica root extract, *IJESD*, 2016, **15**(3), 227–240, DOI: 10.1504/IJESD.2016.077370.

35 G. Muhammad, M. A. Hussain, M. U. Ashraf, M. T. Haseeb, S. Z. Hussain and I. Hussain, Polysaccharide based superabsorbent hydrogel from Mimosa pudica: Swelling-

deswelling and drug release, *RSC Adv.*, 2016, **6**(28), 23310–23317, DOI: **10.1039/C5RA23088H**.

36 U. V. Deore and H. S. Mahajan, Hydrogel for topical drug delivery based on *Mimosa pudica* seed mucilage: development and characterization, *Sustainable Chem. Pharm.*, 2022, **27**, 100701, DOI: **10.1016/j.scp.2022.100701**.

37 S. K. Gangai Abirami, K. Sudha Mani, M. Nisha Devi and P. Nirmala Devi, The Antimicrobial Activity Of *Mimosa Pudica L*, *Int. J. Ayurveda Pharma Res.*, 2015, **2**(1), 105–108. Available: **https://ijapr.in/index.php/ijapr/article/view/289**.

38 K. S. Girish, H. P. Mohanakumari, S. Nagaraju, B. S. Vishwanath and K. Kemparaju, Hyaluronidase and protease activities from Indian snake venoms: neutralization by Mimosa pudica root extract, *Fitoterapia*, 2004, **75**(3–4), 378–380, DOI: **10.1016/J.FITOTE.2004.01.006**.

39 J. Paul, S. Khan, S. Mohammed and S. M. B. Asdaq, Wound healing evaluation of chloroform and methanolic extracts of mimosa pudica roots in rats, *Int. J. Adv. Biol. Biomed. Res.*, 2010, **1**(4), 223–227. Available: **https://www.biomedscidirect.com/**.

40 K. Johnson, G. Narasimhan and C. Krishnan, Mimosa pudica linn-a shyness princess: a review of its plant movement, active constituents, uses and pharmacological activity, *Int. J. Pharma Sci. Res.*, 2014, **5**(12), 5104–5118, DOI: **10.13040/IJPSR.0975-8232.5(12).5104-18**.

41 G. Muhammad, M. A. Hussain, I. Jantan and S. N. A. Bukhari, *Mimosa pudica L.*, a High-Value Medicinal Plant as a Source of Bioactives for Pharmaceuticals, *Compr. Rev. Food Sci. Food Saf.*, 2016, **15**(2), 303–315, DOI: **10.1111/1541-4337.12184**.

42 U. Aziz, R. Akther, M. Shahriar and M. A. Bhuiyan, *In vivo* pharmacological investigation of Mimosa pudica L, *Int. J. Pharm. Pharm. Sci.*, 2024, **6**(2), 66–69, Available: **https://www.researchgate.net/publication/261028237**.

43 M. C. Peng, V. Sethu and A. Selvarajoo, Performance study of chia seeds, chia flour and Mimosa pudica hydrogel as polysaccharide-based superabsorbent polymers for sanitary napkins, *Mater. Today Commun.*, 2021, **26**, 101712, DOI: **10.1016/J.MTCOMM.2020.101712**.

44 S. Yadav, M. P. Illa, T. Rastogi and C. S. Sharma, High absorbency cellulose acetate electrospun nanofibers for feminine hygiene application, *Appl. Mater. Today*, 2016, **4**, 62–70, DOI: **10.1016/j.apmt.2016.07.002**.

45 S. F. Altschul, W. Gish, W. Miller, E. W. Myers and D. J. Lipman, Basic local alignment search tool, *J. Mol. Biol.*, 1990, **215**(3), 403–410, DOI: **10.1016/S0022-2836(05)80360-2**.

46 S. Pradhan, S. Mohanty and S. K. Nayak, In-situ aerobic biodegradation study of epoxy-acrylate film in compost soil environment, *J. Polym. Environ.*, 2018, **26**(3), 1133–1144, DOI: **10.1007/s10924-017-1021-6**.

47 A. El-Latif Hesham, N. Mohamed, M. Ismail, N. H. Mohamed, M. A. Ismail and A. A. M Shoreit, 16S rRNA gene sequences analysis of Ficus elastica rubber latex degrading thermophilic Bacillus strain ASU7 isolated from Egypt, *Biodegradation*, 2012, **23**(5), 717–724, DOI: **10.1007/s10532-012-9547-8**.

48 V. M. Pathak and Navneet, Review on the current status of polymer degradation: a microbial approach, *Bioresour. Bioprocess.*, 2017, **4**, 15, DOI: **10.1186/s40643-017-0145-9**.

49 A. E. Zeenat, D. A. Bukhari, S. Shamim and A. Rehman, Plastics degradation by microbes: a sustainable approach, *J. King Saud Univ., Sci.*, 2021, **33**(6), 101538, DOI: **10.1016/j.jksus.2021.101538**.

50 A. J. Capezza, F. Muneer, T. Prade, W. R. Newson, O. Das, M. Lundman, R. T. Olsson, M. S. Hedenqvist and E. Johansson, Acylation of agricultural protein biomass yields biodegradable superabsorbent plastics, *Commun. Chem.*, 2021, **4**(52), 1–11, DOI: **10.1038/s42004-021-00491-5**.

51 M. C. Peng, V. Sethu and A. Selvarajoo, Performance study of chia seeds, chia flour and Mimosa pudica hydrogel as polysaccharide-based superabsorbent polymers for sanitary napkins, *Mater. Today Commun.*, 2021, **26**, 101712, DOI: **10.1016/J.MTCOMM.2020.101712**.

52 J. Arrondo, A. Muga, J. Castresana and F. M. Goni, Quantitative studies of the structure of proteins in solution by Fourier-transform infrared spectroscopy, *Prog. Biophys. Mol. Biol.*, 1993, **59**(Issue 1), 23–56, DOI: **10.1016/0079-6107(93)90006-6**.

53 M. C. Besteiro, A. J. Guiomar, C. A. Gonçalves, V. A. Bairos, M. N. de Pinho and M. H. Gil, Characterization and *in vitro* hemocompatibility of bi-soft segment, polycaprolactone-based poly (ester urethane urea) membranes, *J. Biomed. Mater. Res., Part A*, 2010, **93**(3), 954–964, DOI: **10.1002/jbm.a.32594**.

54 M. N. Alam, M. S. Islam and L. P. Christopher, Sustainable Production of Cellulose-Based Hydrogels with Superb Absorbing Potential in Physiological Saline, *ACS Omega*, 2019, **4**(5), 9419–9426, DOI: **10.1021/ACSOMEGA.9B00651**.

55 C. R. Reshmi, G. Reshma, S. V. Nair and D. Menon, Superabsorbent sodium carboxymethyl cellulose membranes based on a new cross-linker combination for female sanitary napkin applications, *Carbohydr. Polym.*, 2020, **248**, 116763, DOI: **10.1016/J.CARBPOL.2020.116763**.

56 J. R. Witono, I. W. Noordergraaf, H. J. Heeres and L. P. B. M. Janssen, Water absorption, retention and the swelling characteristics of cassava starch grafted with polyacrylic acid, *Carbohydr. Polym.*, 2014, **103**(1), 325–332, DOI: **10.1016/J.CARBPOL.2013.12.056**.

57 M. Kamal, E. M. Abdelrazek, N. M. Sellow and A. M. Abdelghany, Synthesis and optimization of Novel Chitosan/Cellulose Acetate Natural Polymer Membrane for water treatment, *J. Adv. Phys.*, 2018, **14**(1), 5303–5311, DOI: **10.24297/JAP.V14I1.7183**.

58 F. T. Minhas, S. Farrukh, A. Hussain and M. Mujahid, Comparison of silica and novel functionalized silica-based cellulose acetate hybrid membranes in gas permeation study, *J. Polym. Res.*, 2015, **22**(4), 1–13, DOI: **10.1007/S10965-015-0701-Y/METRICS**.

59 H. N. Lavudi, S. Kottapalli and F. M. Goycoolea, Extraction, purification and characterization of water soluble galactomannans from Mimosa pudica seeds, *Eurobiotech J.*, 2017, **1**(4), 303–309, DOI: **10.24190/ISSN2564-615X/2017/04.07**.

60 Z. Fathi, S. Jahani, M. S. Zandi and M. M. Foroughi, Synthesis of bifunctional cabbage flower–like Ho^{3+}/NiO nanostructures as a modifier for simultaneous determination of methotrexate and carbamazepine, *Anal. Bioanal. Chem.*, 2020, **412**(4), 1011–1024, DOI: **10.1007/S00216-019-02326-8/METRICS**.

61 ASTM G160-12, *Standard Practice for Evaluating Degradation and Microbial Susceptibility of Nonmetallic Materials by Soil Burial*, ASTM International, 2012.

62 G. Goksen, D. Demir, K. Dhama, M. Kumar, P. Shao, F. Xie, N. Echegaray and J. M. Lorenzo, Mucilage polysaccharide as a plant secretion: Potential trends in food and biomedical applications, *Int. J. Biol. Macromol.*, 2023, **230**, 123146, DOI: **10.1016/j.ijbiomac.2023.123146**.

63 N. Das and P. Chandran, Microbial Degradation of Petroleum Hydrocarbon Contaminants: An Overview, *Biotechnol. Res. Int.*, 2011, **2011**, 1–13, DOI: **10.4061/2011/941810**.

64 N. Fujimoto, Bacillus licheniformis Bearing a High Cellulose-Degrading Activity, which was Isolated as a Heat-Resistant and Micro-Aerophilic Microorganism from Bovine Rumen, *Open Biotechnol. J.*, 2011, **5**(1), 7–13, DOI: **10.2174/1874070701105010007**.

65 M. Asif, Z. L. Qun, Q. Zeng, M. Atiq, K. Ahmad, A. Tariq, N. A. Ansari, J. Blom, L. Fenske, H. A. Alodaini and A. A. Hatamleh, Comprehensive genomic analysis of Bacillus paralicheniformis strain BP9, pan-genomic and genetic basis of biocontrol mechanism, *Comput. Struct. Biotechnol. J.*, 2023, **21**, 4647–4662, DOI: **10.1016/J.CSBJ.2023.09.043**.

66 E. M. N. Polman, G. J. M. Gruter, J. R. Parsons and A. Tietema, Comparison of the aerobic biodegradation of biopolymers and the corresponding bioplastics: a review, *Sci. Total Environ.*, 2021, **753**, 141953, DOI: **10.1016/J.SCITOTENV.2020.141953**.

67 I. Zalila-Kolsi, A. Ben-Mahmoud and R. Al-Barazie, Bacillus amyloliquefaciens: Harnessing Its Potential for Industrial, Medical, and Agricultural Applications—A Comprehensive Review, *Microorganisms*, 2023, **11**(9), 2215, DOI: **10.3390/MICROORGANISMS11092215**.

68 O. B. Chukwuma, M. Rafatullah, H. A. Tajarudine and N. Ismail, A Review on Bacterial Contribution to Lignocellulose Breakdown into Useful Bio-Products, *Int. J. Environ. Res. Public Health*, 2021, **18**(11), 6001, DOI: **10.3390/IJERPH18116001**.